MEVTV WORKSHOP ON
THE EVOLUTION OF MAGMA BODIES ON MARS

LPI Technical Report Number 90-04
LUNAR AND PLANETARY INSTITUTE 3303 NASA ROAD 1 HOUSTON, TEXAS 77058-4399

MEVTV WORKSHOP ON

THE EVOLUTION OF MAGMA BODIES ON MARS

Edited by

P. Mouginis-Mark

and

J. Holloway

Held at

San Diego, California

January 15-17, 1990

Sponsored by

Lunar and Planetary Institute

Lunar and Planetary Institute **3303 NASA Road 1** **Houston, Texas 77058-4399**

LPI Technical Report Number 90-04

Compiled in 1990 by the
LUNAR AND PLANETARY INSTITUTE

The Institute is operated by Universities Space Research Association under Contract NASW-4066 with the National Aeronautics and Space Administration.

This report may be cited as:
Mouginis-Mark P. and Holloway J., eds. (1990) *MEVTV Workshop on the Evolution of Magma Bodies on Mars.* LPI Tech. Rpt. 90-04. Lunar and Planetary Institute, Houston. 62 pp.

Papers in this report may be cited as:
Author A. A. (1990) Title of paper. In *MEVTV Workshop on the Evolution of Magma Bodies on Mars* (P. Mouginis-Mark and J. Holloway, eds.), pp. xx-yy. LPI Tech. Rpt. 90-04. Lunar and Planetary Institute, Houston.

This report is distributed by:

ORDER DEPARTMENT
Lunar and Planetary Institute
3303 NASA Road 1
Houston, TX 77058-4399

Mail order requestors will be invoiced for the cost of shipping and handling.

Cover illustration: Oblique view of the martian volcano Olympus Mons, showing the prominent basal escarpment and nested summit caldera. Viking Orbiter image 641A52.

Contents

Preface

On January 15-17, 1990, the Lunar and Planetary Institute, under the auspice of the Mars: Evolution of Volcanism, Tectonism and Volatiles (MEVTV) Program, hosted the Workshop on the Evolution of Magma Bodies on Mars onboard the *William D. Evans* in San Diego Harbor. The workshop focused on many of the diverse approaches related to the evolution of magma bodies on Mars that have been pursued during the course of the MEVTV program. Approximately 35 scientists from the Mars volcanology, petrology, geochemistry, and modeling communities attended.

Segments of the meeting concentrated on laboratory analyses and investigations of SNC meteorites, the interpretation of Viking Orbiter and Lander datasets, and the interpretation of computer codes that model volcanic and tectonic processes on Mars. Via a series of talks, posters, and ample opportunities for discussions, the workshop provided the opportunity for members of these different subdisciplines to interact with each other and to compare their results.

It is likely that most of the participants left the meeting with a new understanding of the interrelationships among the different aspects of magmatic processes on Mars. As the planetary community prepares for the next Mars Data Analysis Program (Mars: Surface and Atmosphere Through Time) and awaits the new data from the Mars Observer mission, the identification and understanding of interrelationships among diverse geophysical processes on Mars are likely to provide stimulating new research

directions over the coming years. The session summaries and the abstracts provided in this volume are the first results of this process to define and interpret such broad interrelationships.

Pete Mouginis-Mark
Honolulu, Hawaii

John Holloway
Tempe, Arizona

Program

Monday, January 15, 8:30 a.m.

Welcome and Logistics

P. J. Mouginis-Mark*
Overview of Volcanological Problems on Mars

J. Holloway
Overview of Petrology/Geochemistry Problems on Mars

INTRODUCTION TO POSTERS

J. C. Aubele*, L. S. Crumpler, S. L. Murchie, J. W. Head, S. T. Keddie, P. C. Fisher, J. Plutchak, A. Selivanov, and M. Naraeva
Preliminary Analysis of Arsia Mons Geology as Characterized by Phobos 2 Termoskan Instrument

S. Baloga*
A Comparison of Theoretical Inferences for Magmatic Supply on Mars

R. G. Burns*
Magmatic Sulfides on Mars

L. S. Crumpler,* J. C. Aubele, and J. W. Head
Calderas on Mars: Implications of Style and History for Subsurface Magmatism

P. Francis*
Is Alba Patera an Analogue of African "Hot Spot" Volcanoes?

R. M. C. Lopes* and C. R. J. Kilburn
Emplacment and Growth of Lava Flow Fields on Earth and Mars

B. K. Lucchitta*
What if Deposits in the Valles Marineris Are Volcanic?

P. J. Mouginis-Mark* and S. K. Rowland
Basaltic Volanoes on Earth

*Denotes speaker

V. Pan* and J. R. Holloway
CO_2 Solubility and Its Implications for Degassing Ascending Magmas

C. Robinson*
Water and Evolving Magma Bodies on Mars

D. H. Scott* and J. M. Dohm
Tectonic Setting of Martian Volcanoes and Deep-seated Intrusives

R. W. Wichman* and P. H. Schultz
A Model of Crustal Subduction by Large Impacts and the Implications for Subsequent Mantle Evolution

Monday, January 15, 1:00 p.m.

SESSION 1: THEMATIC TALKS

C. M. Bertka*, J. R. Holloway, and V. Pan
Martian Mantle Primary Melts

P. H. Schultz* and R. W. Wichman
Contamination of the Martian Mantle by Basin-forming Impactors

J. H. Jones*
Isotopic Relationships Among the Shergottites, the Nakhlites and Chassigny: Implications for Volcanism on Mars

N. G. Barlow*
Relative Ages of Martian Volcanoes

Discussion/Posters

Tuesday, January 16, 8:30 a.m.

SESSION II: THEMATIC TALKS

P. J. McGovern* and S. C. Solomon
State of Stress and Eruption Characteristics of Martian Volcanoes

M. T. Zuber* and P. J. Mouginis-Mark
Constraints on Magma Chamber Depth of the Olympus Mons Volcano, Mars

L. Wilson*
Numerical Modeling of Magma Transport

J. Longhi*
Complex Magmatic Processes on Mars

M. C. Johnson*, M. J. Rutherford, and P. C. Hess
Intensive Parameters of SNC Petrogenesis

D. A. Crown* and R. Greeley
Hadriaca Patera: Evidence for Pyroclastic Volcanism in the Hellas Region of Mars

Tuesday, January 16, 1:00 p.m.

SESSION III: THEMATIC TALKS

F. J. Spera* and D. J. Stein
Rheological Properties of Martian Magmas

J. Crisp*
Constraints on Eruption Rates and Cooling of Three Lava Flows at Alba

Discussion/Posters

Wednesday, January 17, 8:30 a.m.

SESSION IV: THEMATIC TALKS

E. Stolper*
Discussion on the Evolution of Magma Bodies on Mars, Issues, New Directions and Results

P. J. Mouginis-Mark*
Closing Comments

Summary of Technical Sessions

Mars displays abundant evidence of constructional and plains volcanism, and it is likely that landforms produced by explosive volcanism and volcano/ground ice interactions exist along with lava-producing volcanoes. The magma bodies that produced these landforms most likely varied in both space and time as a consequence of the petrologic, tectonic, and thermal evolution of Mars. As the MEVTV Project drew to a close, the goals of the workshop were thus to bring together the perspectives of the experimental petrologists, geochemists, tectonic modelers, physical volcanologists, and geomorphologists interested in the evolution of magma bodies on Mars.

Several themes for discussion were identified before the workshop. These themes included the timescales for magma evolution, the differentiation history of magma bodies and lavas, the internal structure of volcanoes, the depth of origin of magmas, rheological and other physical properties of magmas, and the tectonic setting of magma bodies and volcanic structures. Two introductory reviews of volcanological problems (P. Mouginis-Mark) and martian petrology/geochemistry (J. Holloway) were given to set the context for the current state of knowledge (and uncertainty!). Via two days of oral and poster presentations, discussions were organized to place topics and diverse scientific perspectives in contrast with each other to encourage lively discussion. At the end of the meeting, E. Stolper provided a synopsis of the highlights of the meeting, providing the opportunity for the Mars Observer experiments to be discussed in the context of their potential contributions to furthering our understanding of martian magma bodies.

Two lively poster sessions were held during each of the afternoon sessions, providing the opportunity for the oral presentations to address topics covered in detail by other investigators in their poster presentations. New results from the Soviet Phobos 2 Termoskan instrument reveal details of the sequences of lava flows not previously observed by Viking. These Termoskan data point toward valuable new information relevant to the interpretation of the physical properties of martian volcanoes when the Mars Observer TES instrument returns high-spectral-resolution information from Mars in a few years time. Further observational data using Viking Orbiter high-resolution images were also presented that indicate that the Valles Marineris may have experienced geologically recent mafic volcanism. Studies of the stratigraphy, geomorphology, and spatial distribution of water channels peripheral to the Tharsis province suggest that the origin of the water is best explained by a combination of volcanic thermal heating of regolith ice and especially juvenile water from magmatic activity.

The discussions based upon the oral presentations at the workshop focused on several topics:

(1) Petrology of SNCs, their implications for interior composition, and the age of surface materials on Mars were discussed. The SNCs are igneous rocks. The view presented at the workshop was that the SNC meteorites are young, ranging in age for the igneous formation event from 180 m.y. for Shergotty to ~1.3 b.y. for Chassigny. This conclusion places the sample community at odds with the investigations of the impact crater size/frequency curves, which are frequently used by photogeologists to obtain relative age dates for planetary surfaces. Observations of Mars made from Viking Orbiter images would suggest older ages for areas believed to comprise "young" basaltic flows such as the Tharsis volcanics, which crater counts would suggest typically have ages in excess of 1 b.y. Discussion of the size and location of the impact crater that would have ejected the SNC meteorites off the martian surface failed to reconcile the differences in approach and understanding of the astrophysical and geochemical aspects of this problem.

Substantial inferences can, however, be drawn from the SNC meteorites and their inferred parent bodies. Recently discovered hydrous phases in SNCs give constraints on water content of parental liquids. Melt inclusions indicate that 2-4 wt% of water is required in the intercumulus liquid. This implies that the parent liquids could have contained up to 0.5 wt% water, which will have significant impact on models for the very early (pre-4.3 b.y.) degassing history of Mars. There is no direct evidence for CO_2, but indirectly the high inferred CaO content of the nakhlite parent and substantial light REE enrichment of Nakhlite parent magma both support high CO_2 content in the mantle region.

Results of experiments to determine the melting relations for a volatile-free martian mantle were presented. These experiments provide a reference for comparison with volatile-containing assemblages at low degrees of melting and are probably an accurate

representation of high degrees of melting. It was shown that high degrees of partial melting would produce appropriate liquids for SNC parent magmas. The viscosity of martian basaltic liquids has been measured both at atmospheric and high pressure. A comprehensive model for the effect of entrained crystals and bubbles of magma viscosity was presented.

(2) It was concluded that photogeological observations may prove to be key in resolving the role(s) of volatiles in the evolution of Mars. Identifying which features were produced by pyroclastic volcanism, the importance of hydromagmatic vs. explosive volcanism involving primitive volatiles, and the occurrence of ash flows vs. airfalls all pertain to the degassing history of martian magmas. Results of laboratory experiments were presented showing that the solubility of CO_2 in probable martian basaltic magmas is a strong function of pressure and temperature and is very low at low pressures. This implies that CO_2 degassing could have been a significant driving force for the eruption of basaltic magmas. Knowledge of the eruptive style derived from Viking images may thus constrain estimates of volatile content and vice versa.

The connection between petrogenesis and volatile contents was also considered. If volatiles were present in the source region on Mars, these volatiles would strongly influence the temperature required for melting, the mineralogy of the source region, and the chemical characteristics of the expected magma types.

(3) The importance of magma chamber depth was discussed in the context of the mineral phases in Chassigny (amphiboles imply >1 kbar or ~7 km depth). The issue was raised that such a relatively great depth may make it even more difficult to envision Chassigny coming from Mars. The general consensus was that a crater large enough to excavate material from this depth is highly unlikely to be hidden from view by subsequent burial, due to the intrinsically large diameter implied for a crater of this depth (a few tens of kilometers in diameter?). It was also noted that Chassigny has very light shock features, and so this sample is unlikely to come from close to the center of the crater that ejected the meteorite.

An alternate approach to understanding magma chamber depths on Mars was taken using finite element models of the tectonic evolution of the summit caldera of Olympus Mons. These models imply that for at least one stage of the collapse history of the summit area of Olympus Mons the depth of the magma chamber was less than 16 km beneath the floor of the current caldera. Consistent with this shallow depth, but not a particularly useful constraint for the location of a magma chamber, is the role of olivine in the fractionation of shergottites, which places the fractionation at a depth of <10 kbar (70 km).

However, several aspects of the significance of magma chamber depth were discussed in the open sessions:

(a) Could volatiles escape quiescently, such as at Kilauea on Earth, or were eruptions more explosive due to the lower gravity? Examples of old highland patera volcanoes (Hadriaca Patera and Tyrrhena Patera) were presented to show that early explosive volcanism probably took place on Mars, but for an unknown reason this style of volcanism did not continue until the late-stage formation of the Tharsis Montes and Olympus Mons.

(b) The lesser influence of foam within the ascending magma could have induced density contrasts between the magma and the country rocks and, also due to the lower martian gravity compared to Earth, could decrease the depth at which an explosive eruption could have been initiated.

(c) Thermal evolution of the magma chamber would be affected by the shallow nature of the chamber, since the chamber would cool more rapidly the closer to the surface the magma resided. Depending upon the rate of supply of new magma from mantle depths, and the frequency and volume of eruptions from the chamber, this cooling would influence the degree of fractionation of the original melt and possibly lead to evolved, more silicic magmas being erupted on Mars. The volumes of these silicic melts would most likely have been quite small (a few cubic kilometers) and would not have been sufficient to have produced the friable deposits seen in the Amazonis region that are hypothesized to be silicic ignimbrite deposits.

(d) The composition of the exsolving/escaping vapor phase from the melt would also affect the atmospheric evolution of Mars and the style of volcanism that took place at the surface. On the Earth, water-rich vapors are characteristic of silicic (andesitic to rhyolitic) magmas that commonly erupt explosively in moderate to large volumes. CO_2-rich vapors are characteristically associated with alkalic magmas such as basalts and kimberlites.

(4) The source of the volatiles within the magma was of primary interest to the workshop attendees. If the volatiles were primordial mantle volatiles, then this has implications for long-term planetary differentiation.

SNC isotope chronology does indicate an early melting event. The concept of "subducting" material from the crust via overturning during large cratering events was proposed and considered particularly important in the context of the release of volatiles during volcanic episodes that can now be observed at the surface. Previous models for the release of martian volatiles have drawn on terrestrial values for volatile contents, but they ignore the important role played by plate tectonics in subducting volatile-rich material into the mantle. On Mars, it appears that either the volatiles were released very early in martian history during accretion or they were buried by basin-forming events and subsequently recycled over an extended period of geologic history.

Photogeology could provide key observations for the evolution of volatile input into the atmosphere through time. The geologic record shows that the styles of volcanism changed from early explosive activity to plains volcanism and subsequent effusive eruptions that built the constructs. SNCs are unlikely to provide the full story of the volatile flux on Mars as a function of time due to their restricted range of ages.

P. Mouginis-Mark *J. Holloway*

ABSTRACTS

A COMPARISON OF THEORETICAL INFERENCES FOR MAGMATIC SUPPLY ON MARS Stephen Baloga, Jet Propulsion Laboratory, California Institute of Technology, Pasadena CA 91109

Morphologic and dimensional evidence obtained from the Viking Orbiters suggests that volcanism evolved on Mars on global, provincial and local spatial scales. Such evolutionary changes in the style and magnitude of volcanic eruptions may have been resulted from physical changes in the source of magmatic supply in addition to geochemical or petrologic changes.

The quantitative relationship between the surface expression of effusive volcanism, magmatic supply considerations, and tectonic setting is not completely understood at present for terrestrial volcanoes. However, a number of different theoretical models have been developed to describe magmatic ascent rates in terms of subsurface processes, such as viscous flow through a conduit and magmatic fracture. Concurrently, various theoretical models have been developed to relate lava flow dimensions to discharge conditions at the vent. In principle, a combination of surface emplacement and magmatic ascent models allows one to develop theoretical inferences about magmatic supply from systematic tendencies in the dimensions and morphologies of lava flows and flow fields. In this work, one recent model for the cooling of lava flows is combined with two separate ascent models and the results are used for inferences about the evolution of Alba Patera. As emplacement and ascent models improve, through further theoretical development and terrestrial analog studies, the ability to unravel the history of volcanism on Mars will also improve.

Open Pipe Model of Magmatic Ascent

An elementary approach to magmatic ascent treats the source of supply as a subsurface vessel charged with a pressure P_o. This pressure is sufficent to drive a fluid with viscosity μ through a vertical open pipe of length L and radius R to the surface with a volumetric flowrate Q. Integration of a simple form of the Navier-Stokes equations gives,

$$P_o = \rho g L + 8 \mu Q L / \pi R^4 \qquad (1)$$

indicating that work must be done to overcome gravity in elevating the fluid and to overcome the viscous resistance to fluid shearing. The form of eq. (1), and terrestrial values for basaltic viscosities and radii, indicates that eruptions from shallow magma chambers will be dominated by excess magmatic pressure. In this limit, the eruption rate is not influenced by the value of gravity implying a congruence of terrestrial and martian dimensions (and presumably morphologies). For deeper magma chambers, the model suggests a martian eruption rate that is about a factor of three higher than the terrestrial analog, if it exists.

Mapping of flow features at Alba Patera indicates that there are systematic differences in areal and volumetric discharges between the flank and summit flows. Flow areas systematically diminish as one progresses from the older flank flows to the younger summit flows. Models of lava flow emplacement generally indicate eruption rates for summit flows comparable to quaternary basaltic eruptins (100-1000 m^3/sec). A much larger range (10^3-10^6 m^3/sec) has been associated with more complex flows on the flanks of Alba. These flows might be analogous to prehistoric Columbia River or Icelandic basalts. When eq. (1) is recast in the form

$$\Delta P = 8 \mu Q L / \pi R^4 \quad (2)$$

it is clear that one possible explanation of the flow patterns at Alba Patera is that a significantly deeper source of magmatic supply is associated with the summit flows relative to the source of the flank flows. Alternative explanations include factors such as significant decreases in excess magmatic pressure or temperature or increases in crystallinity. Resolution of preferred alternatives would benefit from independent petrologic or geochemical inferences.

Buoyancy Driven Magmatic Fracture

Another concept for magmatic transport through the lithosphere is by buoyancy driven magmatic fracture [1, 2] through thin cracks with dimensions that have been interpreted as dikes. Unlike the open pipe model, the density difference between the ascending magma and the ambient lithosphere is considered to be the cause of the eruption. The resulting eruption rate is given by

$$Q = 4.7 A (\Delta \rho^4 g^4 w^5 / \rho_m^3 \mu)^{1/7} \quad (3)$$

where A indicates the area of a fissure with width w, Δ p is the density difference and ρ_m is the ambient lithospheric density. Given that the lava flow emplacement models correctly describe the eruption rate tendencies at Alba Patera, eq. (3) suggests the possibility that the later summit flows at Alba were associated with significantly smaller density differences than the flank flows. By inference, the summit flows may have resulted from shallower sources a conclusion opposite to that suggested by the open pipe model.

There are other models for magmatic ascent, such as the propagation of buoyancy-driven solitary waves [3], and numerous variations of these three major themes. Although the underlying physics of different models provides interesting comparisons for volcanic evolution of Mars, independently derived geochemical, petrologic or compostional information is needed to isolate a preferred suite of applicable eruption concepts and quantitative models.

References

1. Spence, D.A. and D.L. Turcotte, Magma-driven propagation of cracks. J. Geophys. Res., 90, 575-580, 1985
2. Turcotte, D.L., A heat pipe mechanism for volcanism and tectonics on Venus, J. Geophys. Res., 94, 2779-2785, 1989
3. Olson, P. and U. Christensen, Solitary wave propagation in a fluid conduit within a viscous matrix, J. Geophys. Res., 91, 6367-6374, 1986

RELATIVE AGES OF MARTIAN VOLCANOES; N.G. Barlow, Code SN21, NASA/Johnson Space Center, Houston, TX 77058.

Several studies have constrained the ages of martian volcanoes based on analysis of superposed impact craters (1, 2, 3, 4). In light of the recent revision of the martian relative chronology in terms of heavy bombardment versus post heavy bombardment formation periods (5), it is instructive to reevaluate the ages of volcanic constructs in order to better chronicle the styles of volcanic activity throughout the planet's history.

The revised chronology differs from earlier studies by using the relative size-frequency distribution plotting technique to analyze crater data. Two types of crater size-frequency distribution curves are seen: a multiple sloped curve found on heavily cratered terrains and a curve approximating a power law distribution function on lightly cratered units. Differences in curve shapes are interpreted in terms of different production populations, with the multiple sloped distribution curve reflective of the heavy bombardment era of impactors and the flatter curve representative of objects dominating the post heavy bombardment period. Units with higher crater density all display the multiple sloped distribution curve, with the transition to the flatter curve occurring at a log R value of approximately -2. Analysis of the size-frequency distribution curves thus leads to a chronology which dates units relative to whether they formed during or after the period of heavy bombardment.

The chronology resulting from this analysis (5) finds that approximately 50% of the planet, located primarily in the southern hemisphere, is covered by terrain units formed during the heavy bombardment period. Another 10%, primarily the ridged plains units, formed near the end of the heavy bombardment period but at a time when impact flux was still high. The remaining 40% of surface units, found largely in the northern hemisphere, have formed since the end of high impact rates.

Many of the individual volcanic constructs have been dated using both relative plots (6) and analysis of crater densities. These techniques indicate that the volcanoes can be divided into five groups based on age. Group I consists of the very young, large shield volcanoes of the Tharsis region (Olympus Mons, Ascraeus Mons, Pavonis Mons, and Arsia Mons). Group II consists of the unique martian volcano Alba Patera. Group III contains some of the volcanoes with steeper slopes: Elysium Mons, Biblis Patera, and Albor Tholus. Group IV consists primarily of the patera (Apollinaris Patera, Tyrrhenna Patera, and Hadriaca Patera) as well as Hecates Tholus and possibly Ulysses Patera. Group V consists of the smaller constructs in the Tharsis region (Uranius Patera, Tharsis Tholus, Ceraunius Tholus, Jovis Tholus, and Uranius Tholus). Groups I and II formed in the post heavy bombardment period based on the shapes of their crater size-frequency distribution curves. Group III straddles the transition from heavy bombardment to post heavy bombardment periods, as indicated by the curve shapes and the similar crater densities to that of the Lunae Planum region which dates from the end of the heavy bombardment period (5) (Table I). Groups IV and V formed during the heavy bombardment period. Neither the curve shapes nor the crater density values can be used alone to constrain the ages of these features, but when used together these techniques provide a valuable way to chronicle the evolution of volcanism on Mars relative to the cratering record.

The five categories outlines above not only describe chronologic groupings but also apparent similarities in eruptive style. This analysis indicates that most of the tholii formed early in martian history, supporting

results of some previous studies (e.g., 3). Formation of these small dome features continued during the time when the highland patera were emplaced, and steep-sided constructs such as Elysium Mons and Biblis Patera formed around the same time that flood volcanism was creating the ridged plains areas. Thus formation of domes and other steep-sided constructs continued throughout much of the heavy bombardment period into the beginnings of post heavy bombardment time. The unique volcano Alba Patera formed in a time when the dominant mode of construct volcanism changed from steep-sided volcanoes to shallow-sloped shield volcanism. The volcanic record on Mars is obviously very complicated, but these observed changes in the morphology of martian volcanoes contain important clues to changes in magma composition and/or style of volcanism over the history of Mars.

References: (1) Blasius, K. R. (1976), *Icarus*, **29**, 343-361. (2) Plescia, J. B. and R. S. Saunders (1979), *PLPSC 10*, 2841-2859. (3) Neukum, G. and K. Hiller (1981), *JGR*, **86**, 3097-3121. (4) Greeley, R. and P. D. Spudis (1981), *Rev. Geophys. Space Phys.*, **19**, 13-41. (5) Barlow, N. G. (1988), *Icarus*, **75**, 285-305. (6) Katz, L. and R. G. Strom (1984), Unpublished data.

Table I

Group	Crater Densities ($\geq$1.5 km/ 10^6 km^2)
I	<500
II	620
III	1100-1200
Lunae Planum	1100-1165
IV	1300-1900
V	>2100

MARTIAN MANTLE PRIMARY MELTS

C.M. Bertka*, J.R. Holloway, and V.Pan Department of Geology, Arizona State University, Tempe, AZ 85287; *also at the Geophysical Laboratory, Carnegie Institution of Washington, Washington D.C. 20008

INTRODUCTION:

Primary melt compositions are liquid compositions in equilibrium with their mantle source region. Models that attempt to predict the diversity of lavas on a planet or outline the petrogenetic history of lavas require information about the chemical and physical properties of primary melts. These properties are determined by the bulk composition, modal assemblage, volatile content, and oxygen fugacity of the source region and by the degree of partial melting.

Most estimates of the bulk composition of the Martian mantle rely on calculations of mantle density. These calculations suggest that the Martian mantle is denser than the Earth's mantle, a difference that is attributed to an iron-enrichment of the Martian mantle(e.g.,1,2,3). Calculations of mantle density depend on knowledge of the mean moment of inertia of Mars. This value is poorly constrained and recently a lower estimate, which would result in a more Earth-like mantle iron abundance, has been proposed (4). However, if Mars is the parent body of SNC meteorites(5) then these samples help constrain the mantle composition independent of estimates of mantle density. Wanke and Dreibus (6) used element correlations between measured ratios in SNCs and chondritic abundances to predict a SNC parent body with a mantle enriched in iron relative to the earth. The purpose of this paper is to present our preliminary experimental phase equilibria and primary melt data for an anhydrous Dreibus and Wanke mantle composition at 10, 20 and 30 kb.

EXPERIMENTAL TECHNIQUE:

Experiments were performed in an end-loaded piston cylinder apparatus with a 0.5" diameter solid-media pyrex-NaCl-alsimag cell assembly. Starting materials were synthesized from spec pure oxides ground under ethanol in an agate mortar for one hour , reduced in a gas mixing furnace (1000° C, fO2 at QFM-1) for 24 hours and reground in a carbide container to less than 5um. Approximately 10 mgs of the starting composition was sealed in graphite-lined platinum capsules. Run duration varied from 24 hours at near solidus temperatures to 1 hour at near liquidus temperatures.

RESULTS:

Preliminary phase equilibria data for the Dreibus and Wanke, (DW) mantle composition at 10, 20 and 30 kb are shown in Figure 1. Experimental Fe/Mg distribution coefficients for ol / opx and gt / cpx pairs in the subsolidus runs are in good agreement with previously determined values (7,8). A spinel lherzolite assemblage is stable to at least 20kb, but the subsolidus spinel phases are less than 10um in size and exhibit variations of up to 7 wt% in aluminum and chrome contents. Mass balance calculations to express the DW mantle composition as proportions of the analyzed subsolidus phases were performed with a least squares fit technique. In all cases the calculated modes duplicate the starting composition with a total error of less than 1.5 wt%, most of which can be attributed to poor spinel analysis.

At 10kb, 1500 C enough melt accumulated at the top of the charge so that the resulting quench crystals + glass material could be analyzed by rastering a 2-um beam across a 20-um x 20-um area. The experimental Fe/Mg ol/melt and ol/opx distribution coefficients also compare favorably with previously determined values (9,7) and mass balance calculations duplicate the starting composition with a total error of less than 0.5wt%. The calculated mode is 51wt% olivine, 4wt % orthopyroxene and 45wt% melt. The composition of this melt, projected on to the planes of the model basalt system olivine-plagioclase-wollastonite-SiO_2, is shown in Figure 3.

DISCUSSION:

Compared to the earlier model Martian mantle bulk compositions, (i.e. Morgan and Anders(2), Goettel(3)), and the proposed terrestrial undepleted mantle samples, (PHN 1611 (10), KLB-1(11)), the DW composition has a greater modal abundance of orthopyroxene (12) (see Figures 2 and 3) largely at the expense of olivine or clinopyroxene. Partial melting of a DW lherzolite assemblage may produce a larger temperature interval of primary melts in equilibrium with only olivine and orthopyroxene. Our data indicates a minimum interval of 200° C at 10kb and 100° C at 20 kb. Experimental data for KLB-1 at 15kb (13) and PHN1611 at 20kb (14) indicate maximum olivine + orthopyroxene + melt intervals of 100 C. The primary melt compositions produced in this interval will be picritic to komatiitic. However, the relative abundance of these primary magma types compared to the tholeiitic and alkali basalt melts expected to be produced at lower degrees of partial melting, before clinopyroxene or the aluminous phase are exhausted, can not be evaluated without additional data. Our previous experimental work (12)

MARTIAN MANTLE PRIMARY MELTS
Bertka, C.M. ; Holloway, J.R. and Pan, V.

suggested that an iron-rich lherzolite assemblage would yield a picritic alkali basalt at small degrees of melting.

Proposed SNC parent magma compositions are shown in Figure 3 along with their closest terrestrial analog , basaltic komatiites(15). An undepleted Dreibus and Wanke mantle composition could yield primary melt compositions with major element abundances similar to model SNC parent magmas. Our 10kb experimental primary melt is similar to "Eg", Shergotty EETA79001A groundmass parental composition (see Figure 3). The experimental composition has a lower calcium content and a higher mg#. Degrees of partial melting less than the experimental 45wt% would produce primary melts with higher calcium contents and lower mg#s. Undepleted Morgan and Anders or Goettel bulk mantle compositions could not yield primary melts which are parental SNC melts.

The surface features of Martian lava flows are often attributed to high eruption rates and/or low viscosity magmas (e.g.,16). Our previous work (17) suggested that the picritic alkali basalt produced at low degrees of partial melting at 23kb has a viscosity of 3 poise at source region pressure; similar in magnitude to its calculated 1atm. values at the same temperature. This viscosity is much smaller than that measured for a terrestrial tholeiite composition at 20kb and near liquidus temperatures, 25 poise(18) but similar in magnitude to 1atm. calculated values for a terrestrial alkali basalt at its 30kb liquidus temperature. Magma ascent rates or crystal fractionation processes in the two planets for any given primary melt type (i.e, alkali basalt, tholeiite,komatiite) may be more sensitive to gravitational differences between the two planets than to viscosity differences between the melts at their respective liquidus temperatures. Additional near solidus phase equilibria data for the model DW Mars mantle should reveal whether or not the bulk composition and resulting modal mineralogy favor the production of low viscosity picritic and komatiitic primary melts.

References. 1) McGetchin, T.R. and Smyth, J.R. (1978) *Icarus* 34, 512-536. 2) Morgan, J.W. and Anders, E. (1979) *Geochim. Cosmochim. Acta* 43, 1601-1610. 3) Goettel, K.A. (1981) *Geophys. Res. Lett.* 8, 497-500. 4) Bills, B.G. (1989) abst. *Lunar and Planet. Sci. XX,* 74. 5) McSween, H.R. (1985) *Rev. Geophys.* 23, 391-416. 6) Wanke, H. and Dreibus, G. (1988) *Phil. Trans. R. Soc. Lond.* A 325, 545-557. 7) Mori, T. and Green, D.H. (1978) *J. Geol.* 86, 83-97. 8) Ellis, D.J. and Green, D.H. (1979) *Contrib. Mineral. Petrol.* 71, 13-22. 9) Roeder, P.L. and Emslie, R.F. (1970) *Contrib. Mineral. Petrol.* 29, 275-289. 10) Nixon, P.H. and Boyd, F.R. (1973) in *Lesotho Kimberlites*, ed. P.H. Nixon. 11) Carter, J.L. (1970) *Geol. Soc. Am. Bull.* 81, 2021-2034. 12)Bertka, C.M. and Holloway, J.R. (1987) *Proc. lunar Planet. Sci. Conf.* 18, 723-739. 13) Takahashi, E. (1985) *J. Geophys. Res.* 91, 9367-9382. 14) Mysen, B.O. and Kushiro I. (1977) *Amer. Mineral.* 62, 843-865. 15) Longhi, J. and Pan. V. (1989) *Proc. Lunar Planet. Sci. Conf. 19th,* 451-464. 16) Schonfeld, E. (1979) abst. *Lunar and Planet. Sci. IX,* 1063. 17) Bertka, C.M, and Holloway , J.R. (1989) abst. *Lunar and Planet. Sci. XX,* 69. 18) Kushiro, I., Yoder, H.S. and Mysen, B.O. (1976) *Jour. Geophys. Res.* 81, 6351-6356. 19) Leshin, L.A., Holloway, J.R., and Bertka, C.M. (1988) abst. *Lunar and Planet. Sci. XIX,* 67

Figure 1. DW Anhydrous Experimental Phase Assemblages

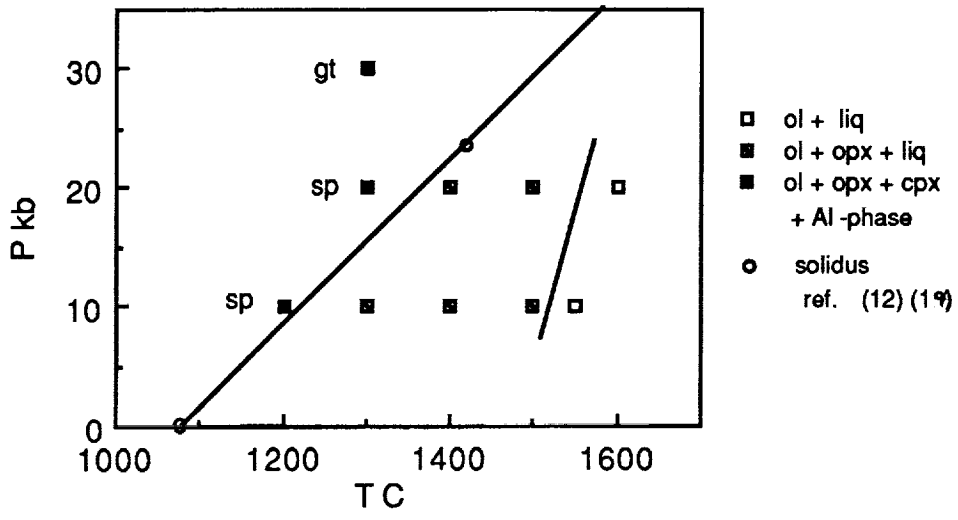

MARTIAN MANTLE PRIMARY MELTS
Bertka, C.M. ; Holloway, J.R. and Pan, V.

Figure 2. Mantle Modes

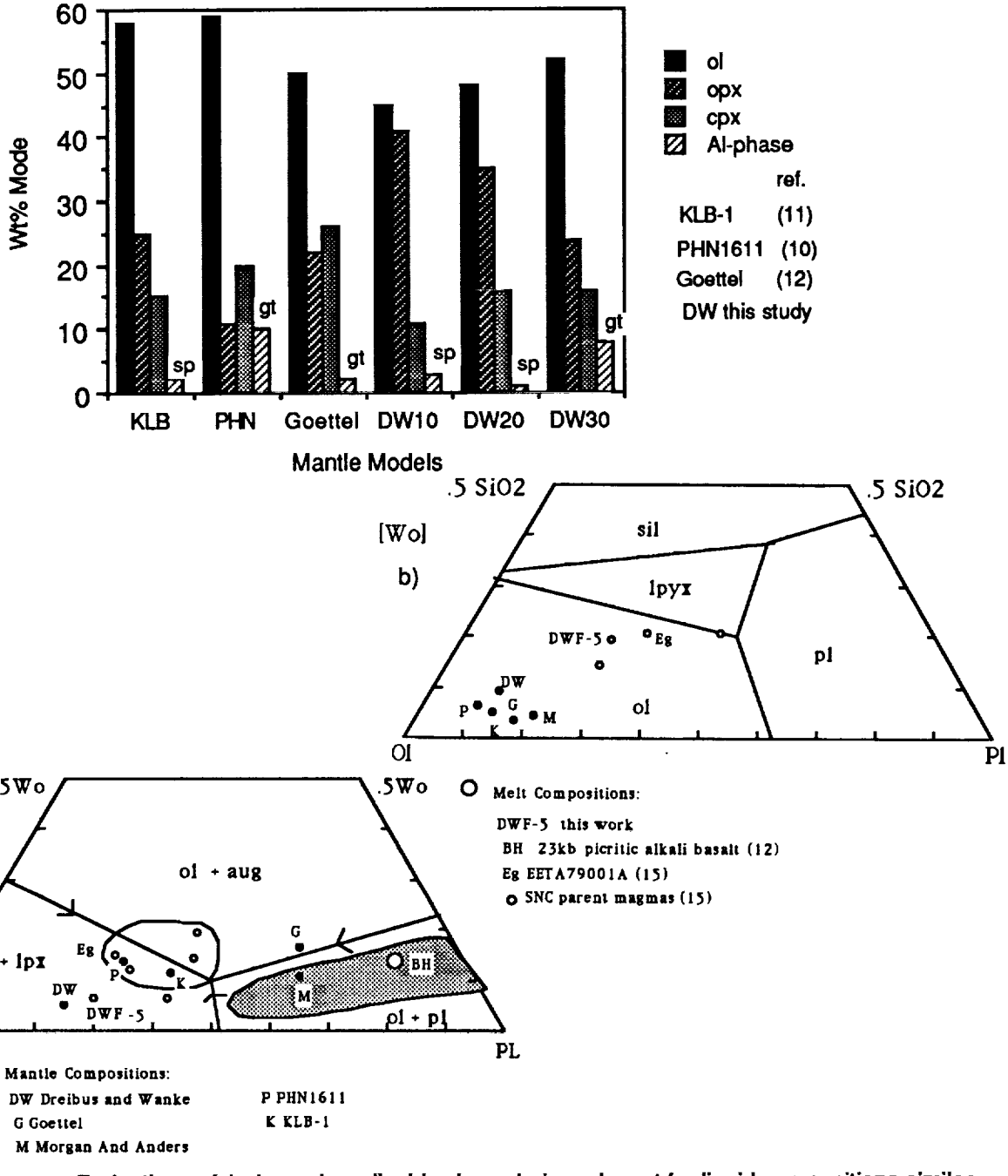

Figure 3 . Projections of 1 atmosphere liquidus boundaries relevant for liquid compositions similar to terrestrial MORBs and SNC parent magmas in mg# and alkali content, after Longhi and Pan (15).

a) Projection from olivine component. Shaded field encloses 5-30kb melts in equilibrium with terrestrial plagioclase- spinel- and garnet- lherzolite assemblages. Dashed line encloses field of terrestrial basaltic komatiite compositions.

b) Projection from Wo component.

MAGMATIC SULFIDES ON MARS

Roger G. Burns, *Department of Earth, Atmospheric and Planetary Sciences, Massachusetts Institute of Technology, Cambridge MA 02139.*

Introduction. Basalts typically contain 0.1-0.2 wt. % sulfur [1]. Shergottite meteorites believed to have originated from Mars rarely exceed 0.2 wt. % S [2]. However, the Viking XRF experiment measured ~3 wt. % S in martian fines [3]. These abundance data summarized in Table 1 for surface materials on Mars pose a dilemma [4]: if the sulfur originated from chemical weathering of basaltic parent rocks, whence did such high concentrations of sulfur in martian regolith originate? One source is SO_2 in volcanic exhalates which, upon reaction with H_2O vapor, produced H_2SO_4 aerosols in acid rain, induced chemical weathering of the surface rocks, and led to the accumulation of sulfate-bearing materials [4].

Another possibility is that deep-weathering reactions of sulfide mineralization associated with underlying ultramafic igneous rocks has generated the oxidized ferric- and sulfate-bearing materials observed on Mars' surface [5]. Clues that these rocks might have been the source of high sulfur contents on Mars are provided by paragenetic relationships between komatiitic basalts and the deduced parent rock-type of martian regolith fines [6,7] and of SNC meteorites [8,9]. On Earth, Archean komatiites host pyrrhotite-pentlandite (± chalcopyrite, pyrite) assemblages which occur as disseminated veins or stratabound lenses at the base of ultramafic flows. The possibility that such Fe-Ni sulfide mineralization occurs in ultramafic and mafic rocks on Mars is examined here.

Since basaltic magma erupting onto surfaces of terrestrial planets such as Mars are partial-melt derivatives of the mantle, properties that need to be evaluated include: (1) the abundance of sulfur in the mantle; and (2) the solubility of sulfur in derived partial melts.

The Sulfur Budget of Mars. Mars probably formed by accretion of carbonaceous chondritic material, so that the abundance of sulfur in the undifferentiated planet would have been ~6 wt. % S. However, core-formation fractionated a considerable proportion of this sulfur into the core; amounts exceeding 15 wt. % S and precluding a solid inner core could explain the apparent lack of a magnetic field on Mars [10]. The observation that SNC meteorites appear to be depleted in several chalcophilic and siderophilic elements has led to the suggestion that such metals are enriched in the sulfur-rich core of Mars, which was estimated to contain 14.24 wt. % S [11]. If the core radius of Mars is assumed to be approximately half the radius of the planet, simple mass balance calculations by the author show that roughly 4.5 wt. % S would remain in the martian mantle after core formation. Therefore, there was probably adequate sulfur remaining in the mantle to be transported to the surface of Mars by magmatic activity.

Sulfur Solubility in Silicate Melts. Experimental measurements [12-17] have demonstrated that the solubility of sulfur in sulfide-undersaturated silicate melts increases with rising temperature, FeO content, and sulfur fugacity, but is reduced by increased silica content, oxygen fugacity, and oxidation of ferrous to ferric iron in the melt. Sulfur solubility is, thus, positively correlated with FeO, TiO_2, MgO and CaO, but negatively with SiO_2, Al_2O_3, Fe_2O_3, Na_2O and K_2O [12]. In sulfide-saturated silicate melts, S solubilities decrease with increasing f_{S2} and decreasing f_{O2}. These trends for S in anhydrous melts are apparent in Table 1 and Figure 1. The effect of increasing pressure, however, remains ambiguous [15-18]. In silicate melts that were equilibrated at oxygen fugacities controlled by the quartz-fayalite-magnetite (QFM) buffer, sulfur predominates as dissolved S^{2-} or HS^- in hydrous magmas [17]. Under more oxidizing conditions corresponding to 2 or more *log* f_{O2} units above the QFM buffer, sulfate species predominate. Compositions of coexisting Fe-Ti oxides in SNC meteorites suggest that they equilibrated under oxygen fugacities near the QFM buffer [2]. Therefore, since SNC meteorites are also volatile-rich [11], the sulfur that was dissolved in parent basaltic melts on Mars probably existed as S^{2-} and HS^-, although a small fraction might have been present as SO_4^{2-} [19].

The ranges of sulfur solubility shown in Figure 1 indicate that melts with 17-22 wt. % FeO (corresponding to compositions of most SNC meteorites and to mafic rocks deduced from XRF measurements of the martian regolith) are saturated with ~0.2 wt. % S at 1200°C. However, the trends suggested by Figure 1 indicate that above 1400°C, an excess of 1 wt. % S could be

dissolved in sulfide-saturated, low Al_2O_3, iron-rich basaltic melts equilibrated at f_{O_2}'s controlled by the QFM buffer.

The Fe/(Fe + Mg) ratio of the martian mantle was deduced to be significantly higher than that of the Earth's mantle **[6,20]**, suggesting that partial melting may have produced iron-rich basaltic magmas with very low viscosities that would possess high sulfur solubilities. Recent experimental measurements suggest that anhydrous martian mantle primary melts formed at a minimum melting temperature of 1400°C at 23 kb contain 23.3 wt. % FeO **[21]**. Melts formed at comparable P and T but containing only 12 wt. % FeO dissolved ~ 0.23 wt. % S **[15]**. The sulfur solubilities in more iron-rich martian melts at high pressures could be much higher, perhaps exceeding 1 or 2 wt. % S in hydrous melts, but would probably be unsaturated relative to the ~4.5 wt. % S calculated earlier to remain in the martian mantle after core formation.

Emplacement of Magmatic Sulfides. Terrestrial komatiites provide clues to the emplacement mechanism of sulfur-rich basaltic magma derived by partial melting of the martian mantle. On Earth during the Archean era when radiogenic heat production was significantly higher than it is now, ultramafic magmas formed by rapid adiabatic emplacement from depths exceeding 200 km were extruded at high temperatures (1350-1700°C). Sulfur saturation of the ultramafic magmas occurred as they cooled near the surface, leading to the separation of immiscible FeS liquids, gravitational settling and riffling out of the sulfides as the lavas advanced over surface depressions, and the formation of pyrrhotite-pentlandite deposits. Very low viscosity komatiitic lavas may have flowed turbulently at high extrusion temperatures accompanied by vigorous convection forces with rapid cooling rates **[22]**. These lavas could also have melted and assimilated large portions of undersaturated sulfur-rich sediments, forming the deep erosion channels into which immiscible FeS liquids subsequently settled.

A similar scenerio has been proposed for Mars **[2,8]**. Close analogies between certain SNC meteorites and komatiites suggest that volcanism on Mars generated ultramafic lava flows and shallow intrusions, and that *in situ* magmatic crystallization produced pyroxene-olivine cumulate rocks represented by nakhlites and chassignites **[8]**. Flows of the nakhlite parent magma were envisaged to have erupted from shield volcanos and flood basalt provinces and to have flowed over rough terrains left by previous flows producing magma lakes in which crystal cumulates were formed. Under these conditions, fractional crystallization of sulfides would also occur, leading to localized concentrations of pyrrhotite-pendlandite assemblages by riffling out from successive flows, although the lower gravitational field on Mars would have inhibited massive ore formation. Eruption of these ultramafic lavas as hot, highly fluid, turbulent melts could also account for the enormous lateral extent of martian flows **[23]**, which might have eroded deep channels on Mars, assimilating early sulfate-enriched duricrust and re-precipitating fresh sulfide deposits in structural depressions.

Evolution of Sulfides on Mars. Magmatic sulfide deposits did not evolve on Mars to the same extent as they have on Earth due to insignificant plate tectonic activity there **[25]**. Interactions of martian mantle with crust, hydrosphere, and atmosphere have been minimal, so that ore deposits such as porphyry copper and molybdenum, granite-hosted mineralization, and sediment-hosted galena-sphalerite assemblages did not form on Mars. Cumulate igneous chromites may occur on Mars, however, as indicated by textures observed in SNC meteorites.

References **[1]** *Basaltic Magmatism on Terrestrial Planets* (1981); **[2]** H.Y.McSween, *Rev. Geophys.*, ***23***, 391 (1985); **[3]** B.C.Clark *et al.*, *JGR*, **87**, 10059 (1982); **[4]** B.C.Clark & A.K.Baird, *JGR*, ***84***, 8395 (1979); **[5]** R.G.Burns, *Proc. 18th LPSC*, 713 (1988); **[6]** T.R.McGetchin & J.R.Smyth, *Icarus*, ***34***, 512 (1979); **[7]** A.K.Baird & B.C.Clark, *Icarus*, ***45***, 113 (1981); **[8]** A.H.Treiman, *GCA*, ***50***, 1061 (1986); **[9]** J. Longhi & V.Pan, *Proc. 19th LPSC*, 451 (1989); **[10]** G.Schubert *et al.*, *4th Intern. Conf. Mars, Abstr.*, 50 (1989); **[11]** G. Dreibus & H. Wanke, *Icarus*, ***71***, 225 (1987); **[12]** D.R.Haughton *et al.*, *Econ. Geol.*, ***69***, 451 (1974); **[13]** D.L.Buchanan & J.Nolan, *Canad. Min.*, **17**, 483 (1979); **[14]** H.Shima & A.J.Naldrett, *Econ. Geol.*, **70**, 960 (1975); **[15]** R.F.Wendlandt, *Amer. Min.*, **67**, 877 (1982); **[16]** M.R.Carroll & M.J.Rutherford, *JGR*, ***90***, C601 (1985); **[17]** *Idem, Amer. Min.*, ***73***, 845 (1988); **[18]** B.O.Mysen & R.K.Popp, *Amer. J. Sci.*, **280**, 78 (1980); **[19]** R. Burgess *et al.*, *EPSL*, ***93***, 314 (1989); **[20]** J.W.Morgan & E.Anders, *GCA*, ***43***, 1601 (1979); **[21]** C.M.Bertka & J.R.Holloway, *Proc. 19th LPSC*, 723 (1988); **[22]** H.E.Huppert *et al.*, *Nature*, ***309***, 19 (1984); **[23]** A.K.Baird & B.C.Clark, *Nature*, ***311***, 18 (1984); **[24]** R.G.Burns & D.S.Fisher, *MEVTV/LPI Tech. Rept.*, ***89-04***, 20 (1989), *JGR*, in press; **[25]** R.J.Floran *et al.*, *Geochim. Cosmochim. Acta*, **42**, 1213 (1978); **[26]** Supported by NASA grants NSG-7604 & NAGW-1078.

MAGMATIC SULFIDES ON MARS: Burns, R.G.

Table 1. Chemical analyses of sulfur-bearing basaltic rocks and melts

	[1]	[2]	[3]	[4]	[5]	[6]	[7]	[8]	[9]
SiO_2	46.5	49.00	44.7	55.5	51.54	39.64	45.6	45.93	41.9
TiO_2	0.2	1.23	0.8	0.4		0.78		3.73	
Al_2O_3	3.6	9.93	5.7	12.0	7.81	29.64	8.75	11.67	11.9
Fe_2O_3	1.0	0.22	18.2					4.06	
FeO	9.4	16.90		9.3	19.50	18.14	12.43	13.36	23.3
MgO	33.0	7.32	8.3	12.6	7.98	0.42	22.95	4.23	12.7
CaO	5.1	11.00	5.6	2.13	11.77	7.73	7.73	8.81	9.4
Na_2O	0.5	1.68	(2.)	4.1		2.64	0.50	2.40	0.8
K_2O	0.2	0.09	<0.3	1.93		0.63		1.28	
others	0.6	1.86	~1.0	0.82				2.07	
S	0.1-0.2	0.22 (0.19)	~2.5-4.0	0.18	0.32	0.245	0.27 (0.47)	0.225 (0.26-0.18)	

[1] Komatiite, Komati, Sth. Africa **[ref.1]**
[2] Shergottite EETA 79001, lith.B. (lith.A: S = 0.19%) **[2]**
[3] Viking XRF analysis **[3,4]**
[4] Chassigny, melt inclusions in olivine **[25]**
[5] Synth. melt, T = 1200°C, $logf_{O_2}$ = -11.50, $logf_{S_2}$ = -3.0 **[13]**
[6] Synth. melt, T = 1350°C, $logf_{O_2}$ = -8.02, $logf_{S_2}$ = -1.06 **[12]**
[7] Synth. ultramafic melt, T = 1450°C, $logf_{O_2}$ = -10.4, $logf_{S_2}$ = -2 (estimated: 0.47% S when $logf_{O_2}$ = -9.2, $logf_{S_2}$ = -0.7) **[14]**
[8] Goose Is. basalt, T = 1420C, P = 20kb, $logf_{O_2}$ = -9, f_{S_2} = 1bar, FeO(melt) = 12 wt,% (At P = 12.5 & 30kb, FeO = 11 & 14%, S = 0.26 & 0.18%) **[15]**
[9] Estimated martian mantle primary melt **[21]**

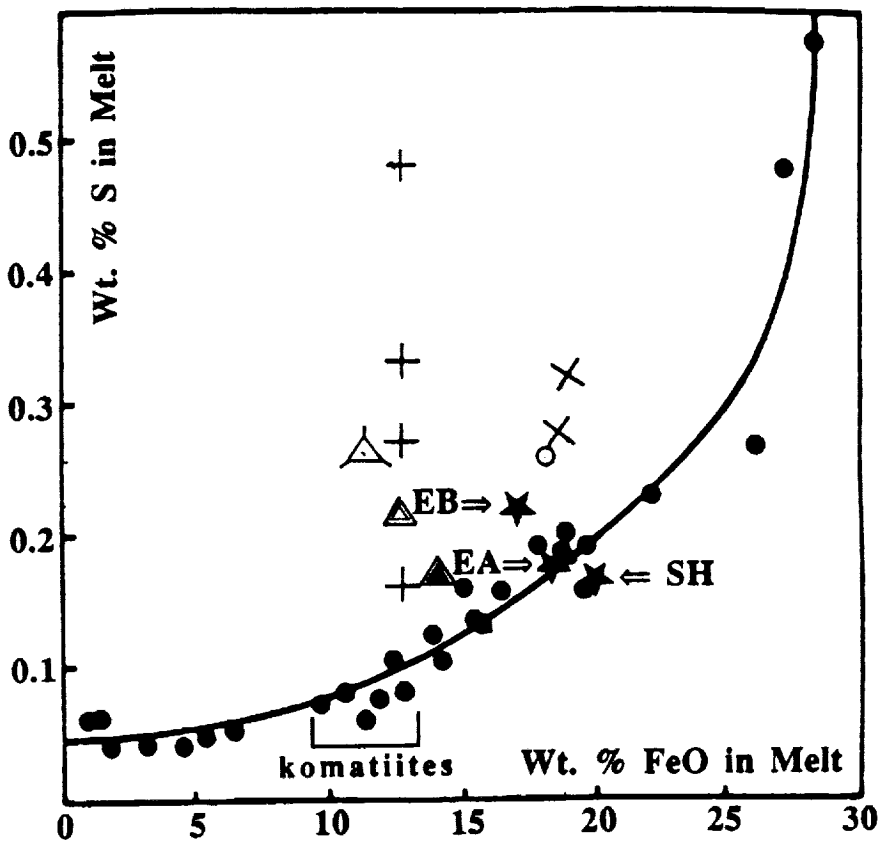

Figure 1. Sulfur solubility versus FeO contents of basaltic melts. ● & O: 1200°C & 1350°C [12]; X: 1200°C [13]; +: 1450°C [14]; ⩚ ◬ & ▲: 1420°C at 12.5 20 & 30 kb [15]; SH = Shergotty; EA and EB = EETA 79001, lithologies A and B [2].

CONSTRAINTS ON ERUPTION RATES AND COOLING OF THREE LAVA FLOWS AT ALBA;
Joy Crisp, Jet Propulsion Laboratory, CalTech, Pasadena, 91109

For three selected lava flows at Alba Patera, there is good agreement between eruption durations predicted by the empirical method of [1] and the two-component thermal model presented in [2]. These flows were chosen because of the extra constraint provided by their thickness profiles, which will be discussed below.

Lava flows on Mars that have flat upper surfaces and show no evidence of central channelization or tube flow have been called sheet flows [3]. Some of these sheet flows are extremely long compared to their widths (15:1-25:1) compared to terrestrial basalt flows [4]. This report focuses on three of these long sheet flows at Alba, L1, L3, and L14 (see Fig.1).

Photoclinometry data provided by P. Davis and J. Plescia show that flow L14 dramatically thickens downstream, from about 60 m to 250 m over its distal 150 km length, whereas two other flows (L1 and L3) have an approximately constant thickness of about 30 m over their distal 60-100 km lengths. This suggests that, during emplacement of L1 and L3, the apparent viscosity of the lava did not increase dramatically with distance from the vent, whereas it probably did increase for L14. The thicknesses of these flows could have been completely controlled by topography, but because of a lack of topographic data it is assumed that this was not the case.

Large increases in viscosity and flow thickness, with increasing distance from the vent, are typical of terrestrial basaltic lava flows. For instance, increasing crystallinity played a key role in the 4 to 5 orders-of-magnitude increase in viscosity of the 1984 Mauna Loa 1A flow [5,6,7]. Most of the viscosity increase and thickening took place in the distal half of the flow. A theoretical modeling study of some of the 1983-4 Puu Oo flows indicates that the increase in viscosity during flow emplacement was about one order of magnitude every two days, and that the increase is better correlated with time than with distance from the vent [8]. Such a relationship is expected if the viscosity increase is a direct result of cooling and crystallization.

Hawaiian basalt undergoes a slight increase in viscosity from 1250°C to 1125°C. Below about 1125°C (≈ 25% crystals) the viscosity increases very quickly as crystallinity increases (e.g., [9]). Thus, a critical temperature of roughly 1125°C can be used as a constraint for the martian flows, assuming that they are basaltic. For different magma compositions, a temperature corresponding to 25% crystallinity can be used [10,11]. To account for their constant thicknesses, Alba flows L1 and L3 should not have cooled below the critical temperature. Flow L14 probably cooled enough during emplacement to develop over 25% crystallinity.

The two-component thermal model developed in [2] can be used to predict the temperature of the inner core of the martian lava flows as a function of time and fraction of exposed core at the surface, f. For values of f between 0.001 and 0.1 (typical terrestrial values), the model predicts that flow L14 had an eruption duration greater than about 3 days (to cool past the critical temperature) and an eruption rate less than 6×10^5 m^3/s. Lopes and Kilburn [1] used an empirical model for terrestrial flows to predict an eruption duration of 21-28 days and an eruption rate of 10^4-10^5 m^3/s for L14. For this duration, the two-component thermal model indicates an $f \approx 10^{-2}$.

Because L1 and L3 did not undergo much thickening, their core temperatures should not have gone below the critical temperature of 25%

crystallinity. With this constraint, the two-component thermal model predicts an eruption duration less than 260 days, and an eruption rate greater than $3x10^2$ m^3/s for L1 and greater than 10^3 m^3/s for L3. Any value of f between 0.001 and 0.1 is consistent with the predicted eruption durations from [1] and with a final core temperature above the critical temperature. The eruption rate estimates for these flows given in [1] are 10^4-10^5 m^3/s. Because the Lopes and Kilburn [1] model predicts that L1 and L3 had higher average velocities than L14, f was probably higher for L1 and L3, on the order of 10^{-1}.

This study shows an example of how theoretical and empirical models can be used to constrain eruption rates and emplacement durations of martian flows. These parameters are crucial for other studies that are concerned with magma ascent from a reservoir at depth or lava flow rheology.

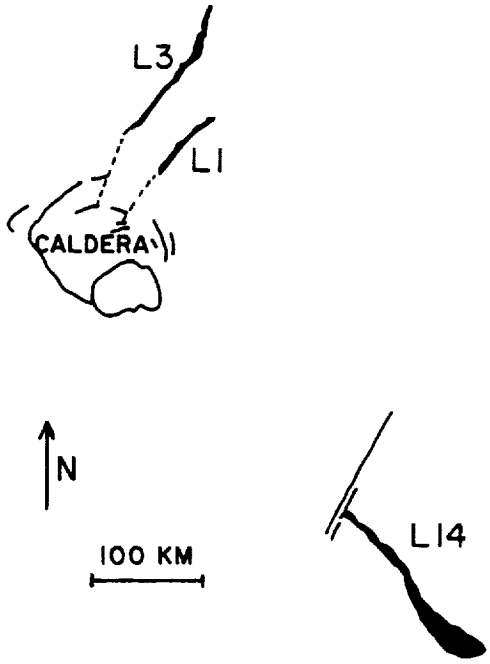

Figure 1. Map showing location of selected lava flows and summit caldera at Alba Patera (map modified from [1]).

References: [1] Lopes, R.M.C. and Kilburn, C.R.J. (1989) Emplacement of lava flow fields: application of terrestrial studies to Alba Patera, Mars, submitted to JGR. [2] Crisp, J. and Baloga, S. (1989) A model for lava flows with two thermal components, J. Geophys. Res., in press. [3] Carr, M.H., Greeley, R., Blasius, K.R., Guest, J.E. and Murray, J.B. (1977) JGR, 82: 3985-4015. [4] Walker, G.P.L. (1973) Lengths of lava flows, Phil. Trans. Roy. Soc. London, A 274:107-118. [5] Lipman, P.W. and Banks, N.G. (1987) U.S. Geol. Survey Prof. Paper, 1350:1527-1567. [6] Moore, H.J., (1987) U.S. Geol. Survey Prof. Paper 1350:1569-1588. [7] Baloga, S.M. (1987) (abstract) EOS, 68:457. [8] Baloga, S., and Crisp, J. (1988) (abstract), NASA MEVTV Program Working Group Meeting: Volcanism on Mars, Oahu, Hawaii, June 27-30, 1988, p.27-29. [9] Shaw, H.R. (1969) J. Petrol., 10:510-535. [10] Ryerson, F.J., H.C. Weed, and A.J. Piwinskii (1988) JGR, 93:3421-3436. [11] Vicenzi, E.P., Ryerson, R.J., and Watson, E.B. (1988) EOS 69:1411.

HADRIACA PATERA: EVIDENCE FOR PYROCLASTIC VOLCANISM IN THE HELLAS REGION OF MARS; ***David A. Crown and Ronald Greeley,*** *Department of Geology, Arizona State University, Tempe, Arizona 85287*

Hadriaca Patera, a large, low relief (< 3 km) volcano located NE of the Hellas basin, was first described as a shield volcano formed by eruptions of low viscosity lavas [1,2]. It is one of the martian highland paterae (areally extensive, low relief volcanoes with central calderas and radial channels and ridges [3]). Four of these features, Hadriaca, Tyrrhena, Amphitrites, and Peneus Paterae, are associated with inferred rings of the Hellas basin [4,5]. Although highland paterae were initially suggested to be basaltic shield volcanoes, a morphometric correlation with terrestrial ash shields was noted [6], and based upon the morphology and erosional characteristics of Tyrrhena Patera, their formation was attributed to phreatomagmatic eruptions as magma encountered the water- or ice-saturated megaregolith [7]. Detailed mapping and analyses of the energetics of eruption and flow processes have shown that the morphology and distribution of units at Tyrrhena are consistent with an origin by the emplacement of gravity-driven pyroclastic flows [8-10]. A large flank flow containing well-defined lava flow lobes and leveed channels, the first definitive evidence for effusive volcanic activity associated with the highland paterae, extends from near the summit of Tyrrhena for over 1000 km to the SW adjacent to Hadriaca.

A geologic map of the Hadriaca region is shown in Fig. 1. Plateau and mountainous materials are regional units [11] which reflect modification of the ancient highland crust. Other prominent features are Dao Vallis and related channeled plains. Volcanic units include the flank flow from Tyrrhena and the caldera-filling and volcanic flank materials of Hadriaca. The caldera at Hadriaca is ~70 km across and filled with smooth, relatively featureless deposits. A well-defined caldera wall is observed to the W and S; to the N and E the caldera wall is not apparent, possibly due to either overflow or mantling by volcanic materials. Within the caldera, scarps are evident and extend into the surrounding flanks of the volcano. Although many of the scarps appear to be erosional, a large scarp near the SW margin of the caldera may be a flow margin of ponded lavas or ash. Surrounding the caldera are the "channeled" flanks of the volcano. Hadriaca is ~290 by 570 km across and asymmetric to the SW, reflecting the slope into the Hellas basin. Flank slopes range from ~0.05° in the N to ~0.60° in the W and S [9]. On the W and S flanks the spacing between the channels is smaller and the number of exposed layers greater than to the N, where the observed scarps (defining the ridges between channels) do not form a distinct radial pattern and only one or two layers are evident. The channels are commonly not continuous along the flanks, and several channels extend from topographic highs such as the rims of small impact craters. In the lower part of the SW flank of Hadriaca, several ridges trending NE-SW and deeper dissection by the channels are observed. No evidence for flank eruptions is apparent. The morphology of the channels and related scarps and the presence of remnants of the ridges suggest an erosional process. The erosional characteristics in combination with the low relief of the volcano and the absence of primary lava flow features favor an interpretation of Hadriaca Patera as ash deposits.

Assuming that eruptions occurred near the present summit region, the dimensions of Hadriaca can be used to constrain possible explosive eruption mechanisms [8,9]. An air-fall origin for most of the deposits can be dismissed because the eruption cloud heights required (comparable to the max. flank width of ~450 km) are unreasonable for the martian atmosphere [12]. Models for the emplacement of gravity-driven flows resisted by a frictional force [13] indicate that the dimensions of Hadriaca require initial velocities as high as 350 - 550 m/sec (for a slope of 0.25° and coefficients of friction between 0.05 - 0.10). Theoretical analyses of hydromagmatic eruptions indicate that these velocities could be produced for <12% conversion of a magma's thermal energy into the kinetic energy of a pyroclastic flow, which is in agreement with experimental results [14]. A magmatic eruption with an exsolved volatile content of > 1%, a mass eruption rate of > 10^7 kg/sec and a 70 km eruption cloud height would also generate sufficient energy [15].

The morphology of the flanks of Hadriaca is consistent with a pyroclastic origin. Quantitative analyses of explosive eruptions indicate that the distribution of units at Hadriaca can be attributed to the emplacement of gravity-driven pyroclastic flows. The location of the volcano in a region containing evidence for volatile-rich surface materials (i.e. Dao and Harmahkis Valles and

related plains) and the absence of this style of volcanism in later periods suggest that groundwater may have driven the eruptions that led to the formation of Hadriaca Patera.

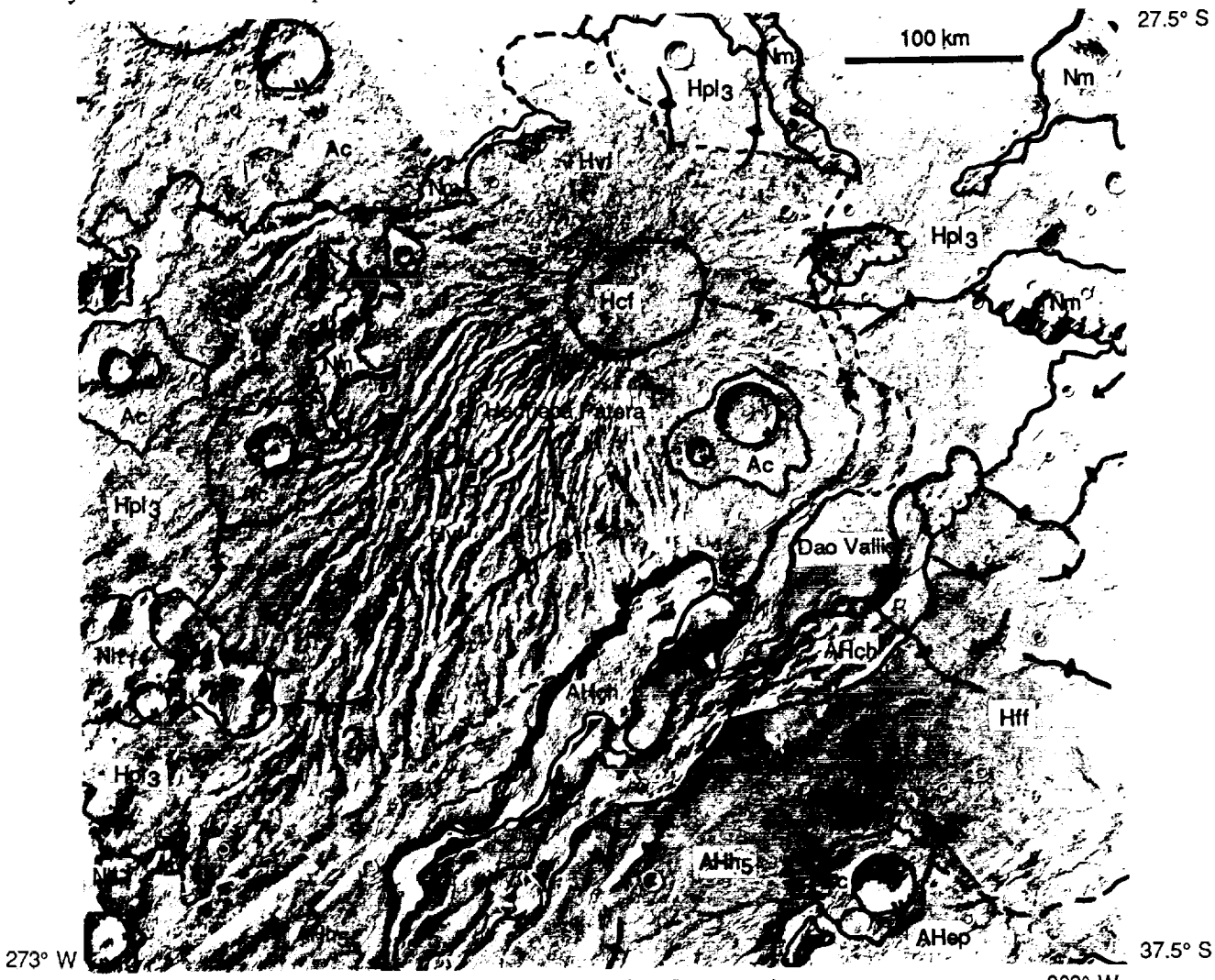

Figure 1. Preliminary geologic sketch map of the Hadriaca Patera region.

Units

Ac	crater materials	Hvf	volcanic flank materials
AHch	vallis floor materials	Hff	flank flow materials
AHh_5	channeled plains materials	Hpl_3	smooth plateau materials
AHep	etched plains materials	Nm	mountainous materials
Hcf	caldera-filling materials	Nh_1	basin rim unit

Map Symbols

- contact
- scarp
- ridge
- channel
- apparent flow direction
- crater rim crest

References: [1] Potter, D.B., 1976, *U.S. Geol. Survey Misc. Geol. Inv. Map I-941.* [2] King, E.A., 1978, *U.S. Geol. Survey Misc. Inv. Series Map I-1073.* [3] Plescia, J.B. and R.S. Saunders, 1979, *Proc. Lunar Planet. Sci. Conf., 10th,* 2841-2859. [4] Peterson, J.E., 1978, *Proc. Lunar Planet. Sci. Conf., 9th,* 3411-3432. [5] Schultz, P.H., 1984, *Lunar Planet. Sci. Conf., XV,* 728-729. [6] Pike, R.J., 1978, *Proc. Lunar Planet. Sci. Conf., 9th,* 3239-3273. [7] Greeley, R. and P.D. Spudis, 1981, *Rev. Geophys. Space Phys., 19,* 13-41. [8] Crown, D.A. and R. Greeley, 1988, *LPI Technical Report 89-04,* 29-31. [9] Crown, D.A., R. Greeley, and M.F. Sheridan, 1988, *Lunar Planet. Sci. Conf., XIX,* 229-230. [10] Greeley, R. and D.A. Crown, 1989, *J. Geophys. Res.*, in press. [11] Greeley, R. and J.E. Guest, 1987, *U.S. Geol. Survey Misc. Inv. Series Map I-1802B.* [12] Mouginis-Mark, P.J., L. Wilson, and J.R. Zimbelman, 1988, *Bull. Volc., 50,* 361-379. [13] Malin, M.C. and M.F. Sheridan, 1982, *Science, 217,* 637-640. [14] Wohletz, K.H., 1986, *Bull. Volcanol., 48,* 245-264. [15] Mouginis-Mark, P.J., L. Wilson, and J.W. Head, 1982, *J. Geophys. Res., 87,* 9890-9904.

CALDERAS ON MARS: IMPLICATIONS OF STYLE AND HISTORY FOR SUBSURFACE MAGMATISM;

L.S.Crumpler, Jayne C.Aubele, and J.W.Head, *Department of Geological Sciences, Brown University, Providence, RI 02912*

Introduction. Calderas on Mars are visible surface volcanic expressions of magmatic processes at depth and offer observational insights into the characteristics of subsurface magmatism. The geological characteristics of calderas are an indirect means of assessing a variety of related parameters such as the volume rate of magma production and movement and the petrologic, geochemical, and isotopic evolution of the responsible magma bodies and the mantle source. For this reason, the study of the physical origins, growth, and modification of calderas is an important volcanological focus on Earth [1] and other terrestrial planets[11].

The primary mechanism of caldera formation is subsidence of a large volume due to the withdrawal of a supporting volume at depth. Within this context, there are fundamental differences among martian calderas in the size, geologic characteristics, and timing of associated events. On the basis of this and recent progress in understanding some of the fundamental factors in the origin and development of calderas in general, we investigate the implications for the nature of magma sources and subsurface magma tectonics of some of the observed differences in large-scale characteristics of martian calderas.

Two Caldera Styles. Two fundamental types of caldera occur throughout the geologic record on Mars as defined on the basis of their geologic and topographic characteristics, particularly of their margins: (1) Simple single scarp-bounded volcanic depressions, and (2) Large-scale concave volcanic depressions or sags with multiple scarps defining their margin. Both types occur on the large and young shield volcanoes as well as on the older highland *patera* type volcanoes.

Olympus-type. The first type is characterized by the summit caldera of Olympus Mons, and includes the calderas of most of the smaller Tharsis and the Elysium shield volcanoes. The overall characteristics of the *Olympus-type* are similar in morphology and apparent structural development to calderas typically associated with central volcanism over a variety of compositions and replenishment rate regimes on Earth. Calderas of this type are characterized by distinct fault-related boundary walls, and often occur in nested and overlapping sets of individual collapse craters, each of generally circular plan shape. Simple calderas of this type on Earth [12] as well as Mars [13] are generally no more than a few tens of kilometers in diameter. A commonly noted characteristic of simple calderas of this type is that the caldera width is of the same order of magnitude as the depth [4] of a significant underlying density contrast. On Earth this commonly correlates with the upper-lower crust seismic discontinuity or the depth to the crust-mantle boundary. On the basis of previous geologic studies of central volcanism on Mars [3,7], the *Olympus-type* calderas on many volcanoes are contemporaneous with flows which erupted and flowed down the flanks of the main shield. Calderas are generally interpreted in these cases to be the result of magma chamber deflation due to eruptions or lateral intrusions of the magma.

Arsia-type. The second (sag-like) type of caldera is characterized by the broadly concave depression on the summit of Arsia Mons. The *Arsia-type* has gently sloping margins rather than the abrupt bounding escarpments characteristic of the *Olympus-type*, occurs characteristically as a single caldera, is more circular, and is larger in diameter than the simple *Olympus-type* calderas. The *Arsia-type* has no directly recognizable counterpart on Earth, although some depressions surrounding broad volcanic regions [6] may be comparable in some respects. In addition to Arsia Mons, the broad summit depression of Pavonis Mons, and the calderas of Apollonaris Patera, Alba Patera, and many of the highland patera may be included in this category. Widths of *Arsia-type* calderas can exceed 100 km on Mars. The formation of calderas of the *Arsia-type* are characteristically late events in several cases on Mars and, in contrast to the contemporaneous timing of the *Olympus-type* with the main period of edifice growth, reflects a major rejuvenation or re-activation after a significant (by crater counts) period of quiescence [3].

Origin and Significance of Two Styles. The formation of calderas of the *Olympus-type* and the underlying associated magma chambers is confined to a narrow range of magmatic production (resupply) rates on Earth [8] and is controlled by the competition between magma replenishment rates, conductive thermal losses, geothermal gradient, wall rock melting temperature, and magmatic flow-through in the individual magma chambers all occurring within the elastic part of the lithosphere [5]. The *Olympus-type* calderas are contemporaneous with flank activity of martian shield volcanoes and are interpreted to be the result of removal of magma either as eruption products or as lateral intrusions within the main shield.

The origin of the *Arsia-type* is not as well constrained because it has not been recognized or studied on Earth. The great width and diffuse gently sloping margins imply a great lateral extent and depth to the source of the differential volume responsible for the subsidence. The depth implied by the *Arsia-type* exceeds estimates [2] of

the equivalent thickness of the elastic lithosphere and approaches plausible estimated depths of magma sources for some martian volcanoes. In this respect, the Arsia-type differs from any recognized calderas on Earth, but may be analogous to some of the larger calderas on Venus [14]. The occurrence of caldera collapse and related eruptions after an extended interval of quiescence reflects a major rejuvenation of volcanism in each case. Although renewed activity of dormant volcanoes occurs on Earth, the large time interval and contrasting style of associated late stage eruptions imply a fundamentally different magmatic style. .

Discussion. On the basis of the variety of ways in which magmas may be generated, several plausible mechanisms that may result in volcanic rejuvenation and the production after a significant lapse in time of the large volumes of magma necessary for the observed eruptions include: (1) renewal of the volcanic thermal source, (2) renewal of (chemical) petrologic source, and (3) slow rates of magma intrusion resulting in late magma chamber formation over extended time at great depth. Mechanism (1) could operate if a punctuated thermal source re-activates the magma system, but fails to explain how or why the thermal source is rejuvenated at each volcano where late renewed activity occurs. The presence of the rejuvenation in several examples, rather than as an isolated case, implies that the process is linked to fundamental processes associated with large central volcanoes on Mars.

Mechanism (3) requires long-term and relatively low volume-rate magma injection at depth. Quantitative volcanologic models of magma chamber formation [5] over a range of probable lithospheric parameters and thermal conditions, and for the low silica and high **Fe** magma compositions plausible for Mars illustrate that magma chambers and associated caldera development on Mars may occur only over short periods in the presence of relatively high magma supply rates in contrast to mechanism (3). Long-term magma production also conflicts with the observed isolated episode of magma eruptions leading to *Arsia-type.*

A variation on mechanism (2), petrologic rejuvenation, shows that the intrusive complex associated with the central volcanism is a potential perturbing chemical inhomogeneity. Because most of the volume associated with eruptions is intrusive [8, 9, 10], a substantial intrusive mass is accumulated over the lifetime of volcano growth [11]. The load resulting from this mass can exceed the long-term strength of the thermally weakened lithosphere, subsidence of the intrusive mass results, and the overburden subsides in a manner analogous to that associated with removal of magma. The temperature of a large volume of relatively low-solidus materials could, after an extended interval of subsidence, exceed the solidus resulting in extensive late eruptions.

Conclusions. Two types of caldera are identified on Mars: (1) Simple calderas resulting from the deflation of relatively high-level magma resevoirs through volcanic eruptions and related magma movements, and (2) large regional subsidence resulting from renewed activity after extended periods of volcanic quiescence. In the second type, the origin of the volume loss responsible for caldera collapse and origin of the relative lateness in the life cycle of central volcanism is unknown. Initial analysis suggests that intrusive loading and subsidence could be a factor in the development of many of the observed characteristics. Assessment of these models is continuing.

References. [1] Williams, H., 1941, Calderas and their origin. *Calif. Uniuv. Publ. Geol. Sci. Bulletin*, **21**, 51-146.; [2] Comer, R.P., S.C.Solomon, and J.W.Head, 1985, Thickness of the lithosphere from the tectonic response to volcanic loads. *Rev. Geophys.*, **23**, 61-92; [3] Crumpler, L.S., and J.C.Aubele, 1978, Structural evolution of Arsia Mons, Pavonis Mons and Ascreus Mons: Tharsis region of Mars, *Icarus*, **34**, 496-511; [4] Gudmundsson, A., 1988, Formation of collapse calderas, *Geology*, **16**, 808-810; [5] Hardee, H.C., 1986, Replenishment rates of crustal magma and their bearing on potential sources of thermal energy. *J. Volc. Geotherm. Res.*, **28**, 275-297 ; [6] Heiken, G., 1976, Depressions surrounding volcanic fields: a reflection of underlying batholiths? *Geology*, **4**, 568-573; [7] Mouginis-Mark, P.J., 1981, Late stage summit activity of martian shield volcanoes. *Proc. Lunar Planet. Sci. Conf.*, **12B**, 1,431-1,447; [8] Shaw, H.R. 1985, Links between magma-tectonic rate balances, plutonism, and volcanism. *J.Geophys. Res.*, **90**, 11,274-11,288; [9] Crisp, J.L., 1984, Rates of magma emplacement and volcanic output. *J.Volc. Geotherm. Res.*, **20**, 177-211; [10] Fedotov, S.A., 1981, Magma rates in feeding conduits of different volcanic centers. *J.Volc. Geotherm. Res.*, **9**, 379-394; [11] Walker, G.P.L., 1988, Three Hawaiian calderas: origin through loading by shallow intrusion? *J.Geophys. Res.*, **93**, 14,773-14,784; [12] Walker, G.P.L., 1984, Downsag calderas, ring faults, caldera sizes, and incremental caldera growth. *J.Geophys. Res.*, **84**, 8,407-8,415.[13] Wood, C.A., 1984, Calderas: a planetary perspective, *J.Geophys. Res.*, **89**, 8,391-8,406; [14] Head, J.W., and L.Wilson, 1986, Volcanic processes and landforms on Venus: theory, predictions, and observations. *J. Geophys. Res.*, **91**, 9,407-9,446.

PRELIMINARY ANALYSIS OF ARSIA MONS GEOLOGY AS CHARACTERIZED BY PHOBOS 2 TERMOSKAN INSTRUMENT;

Crumpler, L.S., Aubele, J.C., Murchie, S.L., Head, J.W., Keddie, S.T., Fisher, P.C., Plutchak, J. (Brown University);
Selivanov, A., Naraeva, M. (Glavkosmos, USSR);

INTRODUCTION. Visible band and thermal IR images returned by the TERMOSKAN instrument on Phobos 2 allows us to characterize the geology of the southern Arsia Mons region of the Tharsis Province of Mars using a new data set and to compare TERMOSKAN observations with Viking IRTM and visible images in an attempt to better characterize the physical properties of geologic and terrain units. The Arsia Mons area is particularly appropriate for this study as it is covered by high-resolution Viking image mosaic data; and the volcanic geology of the area (Crumpler and Aubele, 1978) suggests the presence of a well-defined series of time-stratigraphic units, with distinctive surface physical properties, that are associated with the geologic evolution of Arsia Mons. By analysing and comparing the TERMOSKAN data with mosaics and maps produced from Viking images, each geologic unit can be isolated and its corresponding thermal and physical surface characteristics examined. By clarifying the nature of the geologic units, the nature of the changes in volcanism with time in this region (petrologic, mechanical, etc.), if they occur, may be better understood. For an initial analysis we reduce the problem to the following questions: (1) Are there variations in the actual surface properties that are detectable in TERMOSKAN data; and (2) Are the observed variations in brightness in the thermal image related to any observed geologic characteristics?

DATA. Information used in this comparison includes 8–14 μm thermal images and 0.5–1.1 μm visible images from TERMOSKAN, visible image mosaics from Viking, IRTM data from Viking (Kieffer et al., 1977), and USGS topographic maps of the Arsia Mons region. A brightness temperature map, based on TERMOSKAN data, as well as maps of surface albedo and geology based on Viking images, were prepared especially for this study.

ANALYSIS. Four broad characteristics that can influence the observed brightness temperature of a surface are considered here. These include: (i) surface altitude (which controls surface thermal conductivity and the atmospheric density effects on the balance of advective and radiative loss of surface thermal energy), (ii) surface slope (which controls incident heating per unit area), (iii) surface albedo (which controls surface emissivity, absorption, and reflection of incident heat), and (iv) surface physical properties (thermal inertia affected by the presence of dust and blocks).

CONCLUSIONS. On the basis of preliminary comparison, there is an apparent correlation of altitude and slope with thermal brightness throughout the TERMOSKAN image. Locally, geologic units with distinctive suface albedo and surface physical properties can be correlated with some thermally distinctive units imaged by TERMOSKAN. Examples are geologic map unit R_1, southeast of the main shield and interpreted to be early post-shield lava flows, and geologic map unit Bm, interpreted to be bright mantling material near the summit of the late-stage flank eruption. The digitate flow ends of unit R_2 also correlate with a distinctive thermal brightness unit. Some of these thermal differences may correlate with associated detailed characteristics of the surface such as fine-scale morphological differences between individual flow units, as often occurs between flows of differing age on Earth. High resolution thermal image data compliments the morphologic and geologic evidence for the time-stratigraphic, and potentially petrologic, evolution of the Arsia Mons structure. Continued analysis of the Termoskan thermal data for specific study areas, such as the summit caldera and late-stage flank lava flows, are proving useful in further defining the detailed geologic history of Arsia Mons.

REFERENCES. Crumpler, L.S. and Aubele, J.C., 1978, Icarus 34, 496–511; Kieffer, H.H., et al., 1977, J.G.R. 82, 4249–4291.

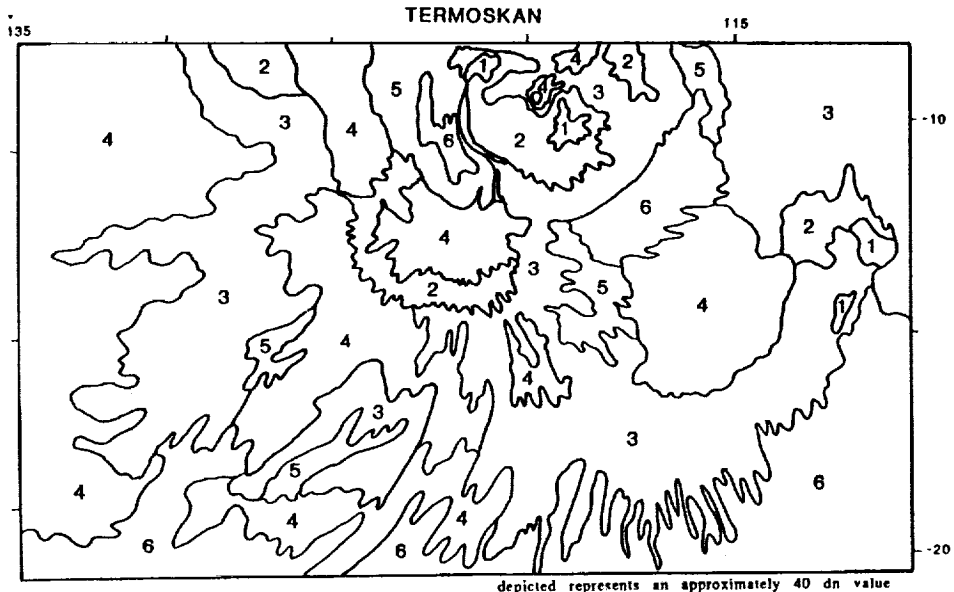

Explanation of TERMOSKAN Map

The original Termoskan image contains an intrinsic west to east gradient in dn values due to atmospheric, oblique viewing, and local solar illumination angle effects. No simple statement of the interpretation of thermal units as mapped can be made, but, in general, each map unit as depicted represents an approximately 40 dn value brightness range. The image is divided into 6 such units (labeled 6 through 1, from lowest to highest dn values respectively). In this preliminary version the west to east gradient is qualitatively removed.

mapped by L.S.Crumpler and J.C.Aubele; base, Photomosaic TERMOSKAN image, Glavcosmos, USSR

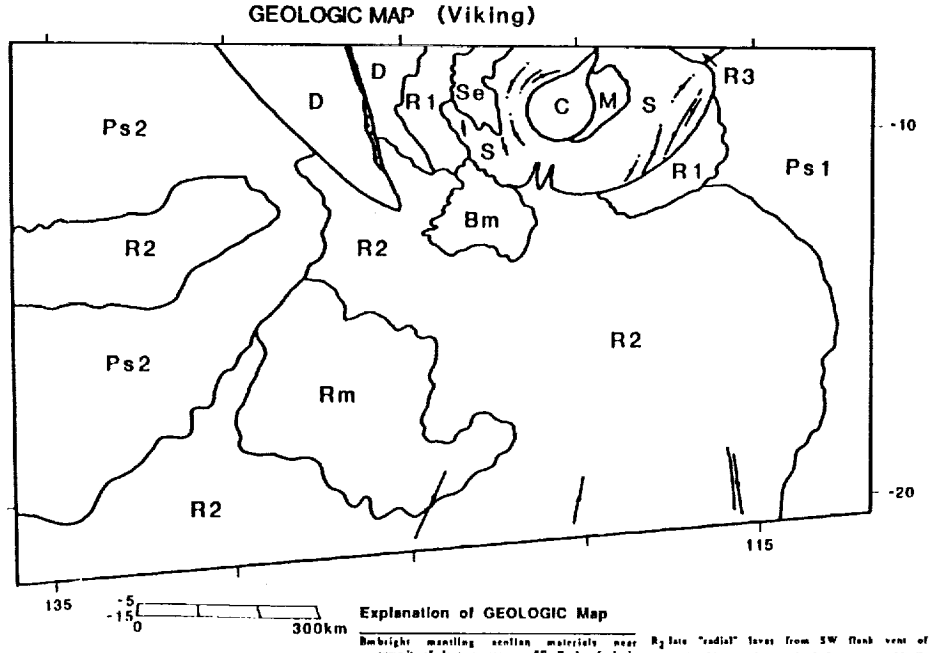

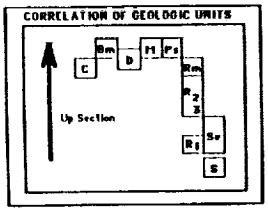

mapped by L.S.Crumpler and J.C.Aubele
map base from Viking mosaic MC-17NW & SW, U.S.Geol.Survey

Explanation of GEOLOGIC Map

Bm bright mantling aeolian materials near summit of lava source on SE flank of Arsia Mons

M mantling deposits on east rim of summit caldera and flank of Arsia Mons

C caldera floor of Arsia Mons

D structurally lineated and disturbed surface west of Arsia Mons interpreted to be a result of gravitational creeping

Ps$_2$ plains streaked on regional (100 km) scale by aeolian mantling deposits

Ps$_1$ plains streaked on local (10 km) scale by aeolian deposits

R$_1$ early "radial" lavas from SW flank vent of Arsia Mons

R$_2$ late "radial" lavas from SW flank vent of Arsia Mons; characterized by topographically distinct flow margins

R$_3$ late "radial" lavas from NE flank vent of Arsia Mons; similar to R$_2$

Rm radial lava surface characterized by indistinct flow margins interpreted to be mantled by regional accumulation of aeolian deposits

S main shield of Arsia Mons consisting of narrow flows and graben concentric to the margins of the central calderas

Se eroded and "etched" lavas on the lower west flank of Arsia Mons

graben

Is Alba Patera an analogue of African 'hot spot' volcanoes?

Peter Francis
Planetary Geosciences
University of Hawaii
2525 Correa Road
Honolulu
Hawaii 96822

Alba and Tyrrhena Paterae are examples of a distinct type of Martian volcanic construct: broad shields of rather low relief. According to recent studies by Cattermole (1987) Mouginis-Mark et al. (1988) and other workers, Alba is 4-500 km in diameter and rises 2-4 km above the surrounding plains. Mouginis-Mark et al. argue from geomorphological considerations that Alba is composed of an outer apron of pyroclastic flows, surmounted in the central regions by a younger carapace of lava flows. Evidence for the lava flows is unequivocal, but the evidence for the older pyroclastic deposits is circumstantial, and rests mainly on their apparently lower resistance to erosion than the lavas and on their thermal inertia characteristics. If genuine, the contrast between early pyroclastic eruptions and younger lava eruptions marks an important change in eruptive style.

Given that there is a significant difference between the upper and lower flanks of Alba, can this be explained without invoking a major change in eruptive style? The 'hot spot' volcanoes of northern Africa may provide instructive analogues. Africa's topography is characterised by broad basins and swells, rather than linear mountain chains. Burke and Wilson (1972) argued that the present topography is due to the fact that Africa has come to rest with reference to the underlying pattern of mantle convection, so that" present relief represents an image of mantle convection where it impinges on the undersurface of the lithosphere" (Burke and Wells, 1989). High ground developes over hotter (mass deficient) mantle and in many places in Saharan Africa has led to surface volcanic activity. Important examples are Hoggar, Tibesti, Darfur and Uweinat. Darfur was described by Francis and Thorpe (1972) and is typical of the mid-plate volcanoes.

The Darfur mountains of western Sudan are a broad elevated region forming a gentle dome 3-400 km in diameter, rising to a maximum of 2 km above the surrounding cratonic basement. A major explosive eruption about 3,000 yr ago formed the Deriba caldera, 8 km in diameter, which represents the youngest event in the evolution of the Jebel Marra volcano (Francis and Thorpe, 1972). A point on the caldera rim marks the highest elevation on the present volcano at 3071 m. Prior to caldera collapse, the volcano may have been much higher. Both pyroclastic flows and basaltic lavas are present in the edifice of the Jebel Marra complex. Reconnaissance fieldwork suggests that the early evolution of the complex was lava dominated and but that the more recent history has been characterised by pyroclastic eruptions.

In the present context, the significance of the Darfur complex is that on the broad scale it presents some important similarities to Alba Patera: the

horizontal and vertical spatial scales are similar, and both structures consist of a younger volcanic assemblage overlying an infrastructure of positive relief. In Darfur, it is clear that the volcanic edifice accounts for only part of the positive relief, about 1.5 km, and that an important component is due to thermal uplift. The oldest rocks beneath Darfur are gneisses affected by the ~525 my Pan African thermal episode. These gneisses were peneplaned prior to the Cretaceous and subsequently buried below a thick cover of continetal sandstones known as the Nubian Sandstone formation of Cretaceous age. The peneplain surface emerges from beneath the Nubian sandstone about 200 km from Jebel Marra, is at an elevation of 1,000 m about 80 km from it, and reaches its maximum elevation beneath the volcano. On satellite images of Darfur, therefore, the volcanic rocks are seen to be overly a basement of Nubian sandstone and crystalline basement rocks, which have sharply different erosional characteristics. Where the volcanics overly sandstone, the latter is much less resistant to erosion, and thus examples of inverted relief are well developed, with lava flows forming prominent ridges.

Could a similar situation prevail at Alba? Could the units underlying the lavas which provide much of the relief be part of the pre-volcano basement? This issue is difficult to resolve without knowledge of the lithospheric thickness beneath the volcano at the time when it formed, and also of how lithospheric thickness subsequently evolved through time. The properties of the Martian lithosphere are not well known, but conventionally it is supposed the present-day lithosphere is extremely thick. Comer et al. (1985) have argued from considerations of the flexural loading of the lithosphere imposed by the volcanic edifice of Alba Patera that the elastic lithosphere was 30 -80 km thick at the time when the circumferential graben formed. Subcontinental terrestrial lithosphere is typically about 125 km thick, but beneath hot spots such as Jebel Marra it may be much less, perhaps only 60 km, due to extension. If the thickness of the elastic lithosphere beneath Alba was of the order suggested by Comer et al., and if further thinning took place over a hot spot, then a component of thermal uplift would also be expected. If thermal uplift did take place, it would decline on mantle cooling, and the volcanic load would be accomodated by flexure, forming the graben surrounding the volcanic construct.

While many aspects of this scenario are debateable, it is at least worth considering as an alternative to the existing model for Alba Patera. If the lavas from Alba overly an elevated basement swell, the materials exposed could include a wide range of lithologies, including older volcanic materials (lavas or pyroclastics), aeolian deposits etcetera. This does not have implications for the origins of the channels on the flanks of the volcano discussed by Mouginis-Mark et al.

References

Cattermole, P., 1987, Geophys. Res. 92, E553-E560. Mouginis-Mark, P.J. Wilson, L and Zimbelman, J., 1988. Bull. Volcanol. 50, 361-379. Burke, K. and Wells, G. L., 1989. Geology, 17, 743-747. Burke, K.C. and Wilson, J.T. 1972. Nature, 239, 387-390. Francis, P.W. and Thorpe, R.S. 1973. Nature,PS, 243, 30-32.~ Comer, R.P., Solomon, S.C. and Head, J.W. 1985. Rev. Geophys. 23, 61-92.

INTENSIVE PARAMETERS OF SNC PETROGENESIS; Marie C. Johnson, Malcolm J. Rutherford, and Paul C. Hess, Dept. of Geological Sciences, Brown University, Providence, RI, 02912

The intensive parameters of SNC petrogenesis are difficult to estimate because the SNC's are cumulate rocks and many of them, *i.e.*, Chassigny and the nakhlites, are virtually monomineralic. Clues to these parameters, however, can be deduced from studying melt inclusions, droplets of melt that were trapped by growing phenocrysts, and combining these data with experimental data. Melt inclusions have been identified in Chassigny, Shergotty, and Zagami (1, 2). The melt in these inclusions has crystallized to varying degrees. Since crystallization occurred in a closed system, the phases should reflect the intensive parameters (pressure, temperature, oxygen and water fugacity) that controlled SNC crystallization. As part of this study, the phases within melt inclusions in Chassigny USNM 624-1 and Shergotty USNM 321-1 were extensively analyzed with an electron microprobe. In addition, phase equilibrium experiments were conducted. One objective was to infer the intensive parameters associated with SNC petrogenesis.

NATURAL MELT INCLUSIONS. Chassigny melt inclusions were trapped by olivine crystals. Most Shergotty melt inclusions were trapped by pigeonite crystals, but some inclusions are found in augite and whitlockite. In both meteorites, the melt inclusions now consist of pyroxenes, amphiboles, oxides, sulfides, phosphates, and glass.

As indicated by previous studies (1, 2), the amphiboles in these inclusions are true kaersutites (>5 wt.% TiO_2) and are hydrous. Core-to-rim traverses across individual kaersutites reveal that they are homogenous. The kaersutites in Chassigny and Shergotty melt inclusions, however, differ (Table 1). A biotite crystal (Table 1) was identified and analyzed in the one of the largest Chassigny melt inclusion. This biotite is extremely titaniferous and has a Mg^* identical to the kaersutite.

Both orthopyroxene and clinopyroxene occur in the Chassigny melt inclusions (Fig. 1). These pyroxenes have homogeneous Fe/Mg ratios, but highly variable Al_2O_3 and TiO_2 contents (Fig. 2). The pyroxenes that coexist with kaersutite are indicated by open symbols and these tend to have the highest Al_2O_3 and TiO_2 contents. Host pigeonites and augites and pyroxenes in Shergotty melt inclusions are also plotted in Fig. 1. The host pyroxenes are zoned with MgO-rich cores and FeO-rich rims, but the pyroxenes in the melt inclusions all have Fe/Mg ratios of ~.78. The melt inclusion pyroxenes have widely varying Wo contents reflecting significant differences in CaO (5 - 15 wt.%). These pyroxenes are similar to the extremely FeO-rich pyroxferrites found in some lunar basalts. Averages of all Chassigny orthopyroxenes and clinopyroxenes are reported in Table 1, and a representative Shergotty pyroxene is also listed.

Most of the oxides in Chassigny both within melt inclusions and in the bulk meteorite are chromites. These chromites have highly variable compositions indicating that they were liquidus phases over a significant crystallization interval. Oxides in Shergotty melt inclusions are ilmenites, magnetites, or hercynites. Ilmenite and magnetite are found in the bulk meteorite but hercynite is not. Hercynite often appears as rims on magnetite cores in the inclusions (1).

The crystalline phases in Chassigny and Shergotty melt inclusions are surrounded by a glassy-looking isotropic phase. This phase tends to be homogenous within a melt inclusion but varies in composition between different melt inclusions. In Chassigny, regions with albite stoichiometry were identified as well as low-SiO_2 rhyolitic glasses (Table 1). In Shergotty, high-SiO_2 rhyolitic glasses were identified (Table 1). These isotropic regions are believed to represent the melt inclusion mesostasis that was shock melted and possibly mixed with other shock melted phases.

Mass balance equations involving the compositions of the Chassigny melt inclusion phases were combined with experimentally determined distribution coefficients to calculate the original trapped melt composition for Chassigny (51% SiO_2, 7.6% Al_2O_3, and 6.5% CaO). The Fe/Mg ratio of this liquid was adjusted to be in equilibrium with Fo_{68} olivine. The major element chemistry of this liquid is a very FeO-rich basalt; the closest terrestrial analogue is a boninite.

DISCUSSION AND CONCLUSIONS. The natural melt inclusion minerals constrain the intensive parameters associated with Chassigny and Shergotty crystallization. These constraints were used to guide the phase equilibrium experiments. For example, two pyroxene geothermometry (using 3)

applied to the Chassigny melt inclusion pyroxenes with the lowest Al_2O_3 contents yields temperatures of 1000°C. For Shergotty, two oxide geothermometry and geobarometry (using 4) indicate that crystallization temperatures were 960° to 930°C, and the oxygen fugacity was 0.5 log units below QFM. Textural and impact excavation studies both indicate that the SNC's are the products of low-pressure crystallization. Therefore, phase equilibrium experiments designed to stabilize kaersutite in equilibrium with different melts were run at 1 and 2 kbar pressures and buffered at QFM. The amphibole liquidus is 960°C consistent with the temperatures indicated by the natural minerals. Once kaersutite begins to crystallize, the melt SiO_2 contents evolve substantially consistent with the high-SiO_2 glasses found in the melt inclusions. The existence of hydrous igneous kaersutite requires that substantial water (>4 wt.%) was dissolved in the coexisting melt (5). Water undersaturated experiments at 2 kbar indicate that the stability field of amphibole plus melt is drastically limited as water fugacity is reduced. These results suggest that water fugacity was at least 940 bars to stabilize amphibole at the temperatures indicated. Mass balance indicates that the liquid trapped initially contained slightly more than 1 wt. % water.

REFERENCES. (1) Treiman, A. H. (1985) *Meteoritics, 20,* 229-243. (2) Floran, R. J. et al., (1978) *Geochem. Cosmochem. Acta, 42,* 1213-1229. (3) Lindsley, D. H.(1983) *Amer. Miner., 68,* 477 - 493. (4) Andersen, D. J. and Lindsley, D. H.(1988) *Amer. Miner., 73,* 714 - 726. (5) Merzbacher, C. and Eggler, D. H. (1984) *Geology, 12,* 587 - 590.

Table 1. SNC melt inclusion compositions.

	SiO_2	TiO_2	Al_2O_3	FeO	MgO	CaO	Na_2O	K_2O	MnO	Tot
					Chassigny					
kaer	39.49	7.00	14.22	10.47	11.53	11.80	2.99	0.33	0.17	98.00
biot	35.71	8.86	13.12	12.12	14.09	0.01	0.17	8.39	0.07	92.55
opx	52.70	0.43	2.86	16.40	25.36	1.61	0.06	0.02	0.50	100.13
cpx	49.70	1.39	4.93	7.64	14.32	20.43	0.58	0.02	0.29	99.74
plag	66.38	0.09	21.07	0.52	0.04	1.19	10.61	0.10	0.00	100.00
glass	71.04	0.18	16.75	0.67	0.06	1.22	5.72	4.37	0.02	100.00
					Shergotty					
kaer	35.15	8.90	15.65	19.79	5.73	11.32	2.32	0.11	0.36	99.31
pyx	47.87	0.50	0.63	38.74	5.86	5.93	0.05	0.00	0.91	100.49
glass	76.66	0.23	12.80	0.95	0.02	1.37	1.96	5.95	0.06	100.00

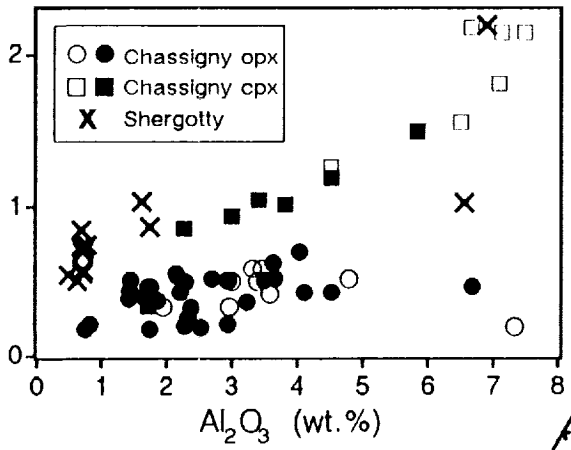

Figure 2

Figure 1

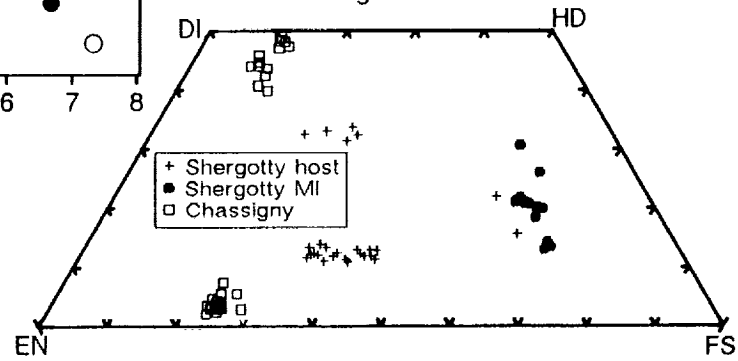

ISOTOPIC RELATIONSHIPS AMONG THE SHERGOTTITES, THE NAKHLITES AND CHASSIGNY: IMPLICATIONS FOR VOLCANISM ON MARS. John H. Jones, SN2, NASA Johnson Space Center, Houston, TX 77058.

Introduction. Isotopic analyses of SNC meteorites have led to diverse interpretations of martian volcanism. One extreme point of view is that the SNC meteorites have an igneous age of ~4-4.5 Æ and that younger ages reflect metamorphic events [1]. The other extreme viewpoint is that metamorphism has had little effect on the isotopic systems of the SNC meteorites because their constitutent minerals all retain normal igneous zoning profiles. If true, the implication is that internal isochrons represent real igneous ages, implying that the nakhlites and Chassigny crystallized at ~1.25 Æ and that the shergottites are only ~200 m.y. old [2]. One intermediate point of view is that all the SNC's have a ~1.25 Æ igneous crystallization age, but that the shergottites' internal isochrons have been reset by later metamorphic events [3]. Another intermediate viewpoint is that the shergottites have a variety of igneous crystallization ages, but that they were metamorphosed or remained as open systems until about 200 m.y. [4]. Essentially, all the investigators of SNC chronologies have arrived at very different conclusions.

A corollary of the second scenario, which predicts very recent volcanism on Mars, is that the shergottites were generated by some sort of mixing process [2]. Mixing, such as magma mixing or assimilation, is necessary to explain the ~1.25 Æ Sm-Nd whole-rock "isochron" for the shergottites [3]. The reason this Sm-Nd "isochron" is believed to be a mixing line is that a similar "isochron" in the Rb-Sr system yields an "age" of ~4.5 Æ [3]. The non-concordance of these two isotopic systems argues strongly that neither has true age significance [2].

Were the shergottites produced by mixing? If, indeed, mixing has been important in the petrogenesis of the shergottites, then there may still be some evidence of that mixing within the shergottite suite. For example, if the shergottites formed at about the same time from an isotopically homogeneous mantle, then it is possible that a regression of the initial isotopic signatures of the shergottites will contain the isotopic composition of the martian mantle at that time. The only reason for this not to be true is if the mixing occurred between more endmember components than there are shergottites. In other words, if the components in the mixing process are not too numerous, the *starting composition* of the shergottites will be contained in a regression of their initial isotopic signatures, regardless of how extensive mixing/assimilation has been [5].

A relevant question is whether an independent estimate of the isotopic composition of the martian mantle can be derived. Here, the nakhlites and Chassigny will be used to formulate an estimate of the mantle's isotopic composition, independently of the shergottites. With this estimate of the isotopic composition of the martian mantle, it is then easy to see if that isotopic composition lies on the shergottite regression plane (or hyperplane). If it does, then the shergottites may come from a common source. If not, then the model fails.

A model mantle for Mars. To make an estimate of the isotopic composition of the mantle source region, the time that the shergottites were removed from that source must be known. For the purposes of this exercise, that time is taken to be 180 m.y. [2]. Also, if the nakhlites and Chassigny are used to arrive at an independent estimate of the martian mantle at 180 m.y., then the time that they were removed from the mantle reservoir must also be known. Here, that time will be taken to be 1.25 Æ. Further, to extrapolate from 1.25 Æ to 180 m.y. requires the additional assumption that the martian mantle was originally homogeneous and that the same mean elemental ratios that existed from the time of the planet's formation until 1.25 Æ in the source region of the nakhlites and Chassigny also pertained up until the time of extraction of basaltic magma from the shergottite source region. This model is shown schematically in Figure 1. The isotopic composition of the martian mantle at 4.5, 1.25 and 0.18 Æ is given in Table 1. The elemental ratios necessary to produce this sequence of isotopic compositions are given in Table 2. The isotopic and elemental characteristics of the mantle described in Tables 1 and 2 are that of a reservoir that was depleted by an early differentiation event.

Figure 1

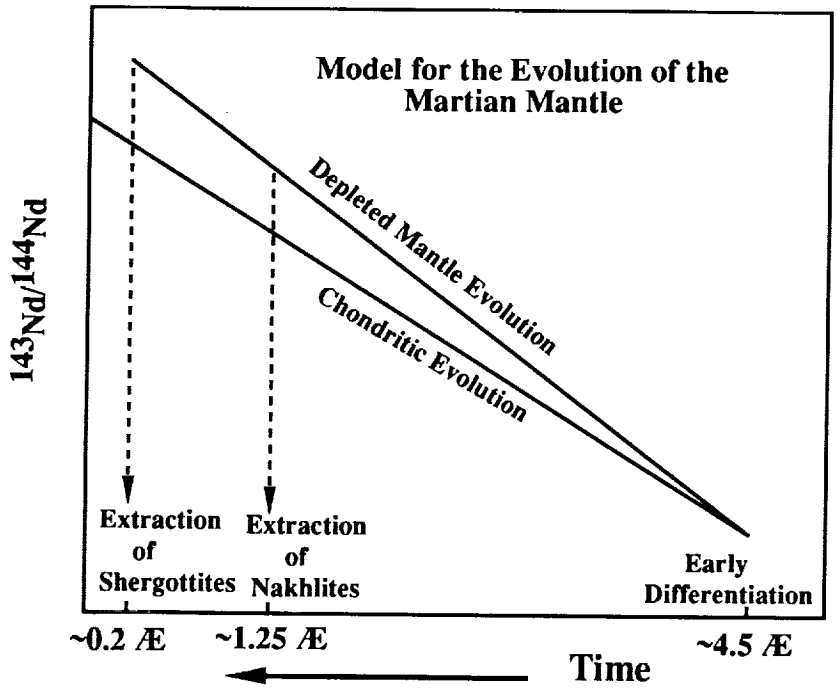

Comparison of the model martian mantle to the shergottites. To compare the model mantle to the array of shergottite data, a hyperplane has been determined from the initial isotopic ratios of the shergottites using ε(Nd) as the dependent variable and $^{87}Sr/^{86}Sr$, $^{206}Pb/^{204}Pb$ and $^{207}Pb/^{204}Pb$ as the independent variables. In other words,

$$\varepsilon(Nd) = a_0 + a_1 (^{87}Sr/^{86}Sr) + a_2 (^{206}Pb/^{204}Pb) + a_3 (^{207}Pb/^{204}Pb)$$

where the a's are the hyperplane constants. Because there are only four shergottites, the hyperplane is uniquely determined. Given the equation for the hyperplane, the $^{87}Sr/^{86}Sr$, $^{206}Pb/^{204}Pb$ and $^{207}Pb/^{204}Pb$ ratios of the model martian mantle at 180 m.y. can be plugged into the equation, ε(Nd) can be calculated and compared to the value estimated from the nakhlites. The ε(Nd) of the model martian mantle is 21.3. For comparison, the ε(Nd) calculated from the hyperplane equation is 20.4-19.0, depending on whether the Pb data of [6] or [1] are used, respectively. Thus, the model mantle does not fall on the hyperplane but plots very close to it.

If the stringent requirement that the model martian mantle fall on the hyperplane is relaxed slightly, the model mantle can be included in the shergottite data set and the five data points can be *regressed.* If the Pb data of [6] are used to calculate the mantle composition, the hyperplane through the data set fits all data to within 0.1 ε units, except for ALHA77005 which differs by 0.3 units. If the Pb data of [1] are used instead, the errors are somewhat larger, but all points still fall within 0.6 ε of the hyperplane. By most standards this is very good agreement, suggesting that the shergottites could indeed have had a common parent that was isotopically similar to the martian mantle at 180 m.y. The selection of ages for the shergottites is crucial to the success of this exercise. If, for example, an age of 360 m.y. for the shergottites had been used instead [4], the exercise fails badly. A more detailed discussion of these results can be found in [5]. These conclusions are similar to those of [7].

Although the model described here is permissive of a relationship among the different groups of SNC meteorites, it is important to note the difficulties the model faces. The most

obvious failing is that there is no ready explanation for the correspondence in ages between the internal isochrons of the nakhlites and the whole rock isochron of the shergottites. As discussed above, the shergottite whole-rock Sm-Nd isochron is interpreted to be a mixing line with no clear-cut age significance. Therefore, in this model, the similarity of the nakhlite ages to the whole-rock Sm-Nd isochron age of the shergottites is viewed as coincidental, in agreement with the U-Pb study of [1].

A more subtle, but perhaps more serious, difficulty is the Sm-Nd ratio of EETA79001, one of the most "primitive" shergottites in terms of its ε(Nd) value. The Sm/Nd ratio of EETA79001 is very high (~2X) compared to that estimated for the martian mantle. If the model is correct, then a major Sm-Nd fractionation, quasi-contemporaneous with the time of the formation of the shergottites, is necessary.

Summary. The results of this exercise reinforce the idea that the SNC meteorites are all young volcanics and have not undergone extensive resetting of their various radiometric chronometers [2]. If so, martian volcanism has continued until very recent times and may be active today. If the model is correct, some portions of the martian mantle may have retained the chemical signatures of an early differentiation event, unmodified, until very recent times.

Table 1
Isotopic Evolution of the Martian Mantle

Age (Æ)	ε(Nd)	$^{87}Sr/^{86}Sr$	$^{206}Pb/^{204}Pb$	$^{207}Pb/^{204}Pb$	$^{208}Pb/^{204}Pb$
4.5	≡0	0.69898	9.307	10.294	29.476
1.25	15.9	0.70254	11.16-11.25	11.50	31.26
0.18	21.3	0.7036	11.59-11.69	11.51	31.79

Table 2
Chemical Parameters of the Martian Mantle

$^{147}Sm/^{144}Nd$	$^{87}Rb/^{86}Sr$	$^{238}U/^{204}Pb$	$^{232}Th/^{204}Pb$
0.234	0.0756	2.78-2.89	10.1

References. [1] Chen J.H. and Wasserburg G.J. (1986) *Geochim. Cosmochim. Acta* **50**, 955-968. [2] Jones J.H. (1986) *Geochim. Cosmochim. Acta* **50**, 969-977. [3] Shih C.-Y., et al. (1982) *Geochim. Cosmochim. Acta* **46**, 2323-2344. [4] Jagoutz E. and Wänke H. (1986) *Geochim. Cosmochim. Acta* **50**, 939-953. [5] Jones J.H. (1989) *Proc. Lunar Planet. Sci. Conf. 19th.* pp. 465-474. [6] Nakamura N., et al. (1982) *Geochim. Cosmochim. Acta* **46**, 1555-1573. [7] Jagoutz E. (1989) *Geochim. Cosmochim. Acta* **53**, 2429-2441.

COMPLEX MAGMATIC PROCESSES ON MARS; J. Longhi, Lamont-Doherty Geological Observatory, Palisades, NY 10964

The SNC (shergottites-nakhlites-Chassigny) meteorites reveal a surprising diversity of magmatic styles on their parent body, which the weight of evidence suggests is Mars (1). There is evidence for large scale mantle heterogeneities, multi-stage melting, extreme fractionation of REE, assimilation of a long-term light REE-enriched component (a 'granitic' crust?), mantle metasomatism, and possibly CO_2-fluxed melting. In some respects the style of martian magmatism is intermediate between that of the Moon and the Earth, however, the terrestrial end-member has more of the character of hot-spots and continental rifts than mid-ocean ridges.

Estimates of the major element composition of the SNC parent magmas show them to be hpyersthene-normative, high-Fe, low-Al liquids (2). As might be anticipated, calculated densities of these liquids are high (2.75-2.96) and viscosities are low (4-128 poise). Figure 1 illustrates these liquid compositions projected from the Olivine component onto the Opx-Pl-Wo plane. The liquidus boundaries are appropriate for this general class of compositions at low-pressure; arrows show direction of decreasing temperature. The diagram is consistent with the petrography: olivine and pyroxene crystallize early, plagioclase crystallizes late (1); this crystallization pattern is different from terrestrial MORB's and continental tholeiites in which plagioclase crystallizes early. The range of projected SNC parent magma compositions is similar to but somewhat more extensive than those of lunar mare basalts and terrestrial basaltic komatiites; the shergottite members of the suite are also generally similar to the soil composition (V) at the Viking Lander sites (3). The shaded area in Figure 1 represents the range of liquids produced by a few percent partial melting of a four-phase terrestrial mantle peridotite (ol-opx-cpx-Al-phase [plag/sp/gar]) at high pressure. Both increasing pressure and increasing alkalis shift liquids to the right in this field. A martian mantle melt (BH) in equilibrium with ol-opx-cpx-gar at 23 kb (4) also lies within this field. In order to produce liquids that project into the area of the SNC liquids, it is necessary to do large degrees of partial melting (~50%) of relatively undepleted mantle or smaller degrees of partial melting of a source depleted in Al. Geochemical and isotopic data discussed below show the latter to be the case. This depletion may be accomplished by the accumulation of olivine and pyroxene (lunar style) or extraction of basalt (terrestrial style).

Figure 2 illustrates some important aspects of SNC trace element and isotopic composition. Figure 2A shows the REE concentrations of two calculated parent liquid compositions for Nakhla. Chassigny parent liquids have similar patterns. Nakhla is an unusual rock consisting of large cumulus augite and minor olivine crystals set in a rapidly crystallized matrix (5). The 'closed system' calculation assumes that no net changes in the intercumulus liquid took place after accumulation of the pyroxene, but does allow for partial equilibration of the cumulus crystals and trapped liquid. The 'open system' calculation is a direct calculation based upon the composition of Nakhla augite (6) and the partition coefficients of (7); this calculation allows for the possibility of migration of intercumulus liquid. Both patterns are similar and show dramatic light REE enrichment. This fractionation is truly remarkable in light of the ε_{Nd} value of +16 (6) which requires that the source had a long term pattern of light REE depletion, i.e. something similar to the EETA79001A pattern in Fig. 2B. Compounding the situation is the low Al content of the Nakhla parent liquid (N) evident in Fig. 1 (Pl is the Al bearing component). The Al content is sufficiently low that garnet, which is the most effective REE fractionating agent, cannot have been a residual phase in the parent magma's source region; niether is there much allowance for removal of augite at low pressure. The problem of deriving strongly light-REE enriched magmas from light-REE depeleted source regions is common to terrestrial hot spots, such as Hawaii (8). Single-stage models require prohibitively small degrees of partial melting (<1%), so multi-stage melting models have been invoked to spread the REE fractionation over two or more steps (e.g., 9). Some sort of multi-stage melting process thus seems necessary to explain the Nakhla parent magma composition with the condition that garnet not have been a residual phase in the last stage of melting. The unusually high Wo content of N (Fig. 1) requires either that the source was dominated by augite or that CO_2, which has the potential of drastically increasing the CaO content of melts coexisiting with olivine and pyroxene, fluxed the melting at pressures > 25 kb (2). Since partial melting of pyroxene dominated sources produces small negative Eu anomalies in the liquid (10) and since there is no evidence of such an anomaly in Fig. 2A, the presence of CO_2 in martian melting processes must be seriously considered.

Fig. 2B illustrates very different REE patterns for the shergottites. The Shergotty pattern is the 70% ICM model taken from (11). The EETA79001A pattern is the bulk rock analysis of (12). EETA79001A is a fine-grained basaltic rock with 10-15 % mafic xenocrysts (13). These xenocrysts will likely have only a minor diluting effect on incompatible elements, so the pattern in Fig. 2B is believed to close to, albeit slightly lower and steeper than, the true parent liquid pattern. The crystallization ages of the shergottites are controversial because of variable shock effects on the isotopic systems and consequentlythe values of ε_{Nd} are model dependent. The values shown in Fig. 2B are consistent with the 180 m.y. age advocated by (14). This age is chosen here because only the younger ages, which yield $\varepsilon_{Nd} > 0$, are petrologically reasonable, and because the 350 m.y. age reported by (15) has been shown to be a mixing line (11). Given these qualifications, projection point (E_g in Fig. 1), the REE pattern, and ε_{Nd} of EETA79001A have a straightfoward explanation: partial melting of a low-Al source region with a long term light-REE depletion. In this regard, the source region was similar to that of Nakhla although the EETA79001A magma genesis was apparently much simpler. The ε_{Nd} values for Nakhla and EETA79001A are much higher than typical terrestrial basaltic values, but are more typical of lunar mare basalts. This similarity suggests that Mars was more

like the Moon in its ability to maintain long term isotopic heterogeneities in its mantle. Lack of crustal recycling on Mars and/or less vigorous mantle convection than the Earth are probable explanations.

Given the similarity of mineral compositions in Shergotty to those in the groundmass of EETA79001A, it is likely that their parent magmas lay along similar liquid lines of descent, as suggested by Fig. 1, and hence they were derived from similar primary magmas and source regions. If so, then REE pattern and ε_{Nd} of the Shergotty parent magma in Fig. 2B are readily explicable as those of a magma derived from a depleted source region like EETA79001A, but subsequently contaminated by a low-temperature, long-term, light-REE enriched component. The slight U-shape in the light REE is especially indicative of such a contamination. This component probably is crustal, but whether it is older basalt, like the Nakhla parent magma (Fig. 2A), or 'granitic' is not clear; the physics of assimilation favors an evolved composition with a low melting point, however. One thing that is clear is the absence of a negative Eu-anomaly in the Shergotty REE pattern. Consequently, this crustal component was unlike lunar KREEP, which has a prominent negative Eu-anomaly (16).

REFERENCES: (1) McSween, H. Y. (1985) *Revs. Geophys., 23*, 391-416. (2) Longhi, J. and Pan, V. (1989) *Proc. Lunar Planet. Sci. Conf. 19th*, p. 451-464. (3)Toulmin, P., III, Baird, A. K., Clark, B. C., Keil, K., Rose, H. J., Jr., Christian, R. P., Evans, P. H., and Kelliker, W. C. (1977) *J. Geophys. Res. 82*, 4625-4634. (4) Bertka, C. M. and Holloway, J. R. (1988) *Proc. Lunar Planet. Sci. Conf. 18th*, 723-739. (5) Treiman A. H. (1986) *Geochim. Cosmochim. Acta, 50*, 1061-1070. (6) Nakamura, N., Unruh, D. M., Tatsumoto, M. and Hutchinson, R. (1982) *Geochim. Cosmochim. Acta, 46*, 1555-1573. (7) McKay G., Wagstaff J., and Yang S.-R. (1986) *Geochim. Cosmochim. Acta, 50*, 927-937. (8) Chen C.-Y. and Frey F.A. (1985) *J. Geophys. Res., 90*, 8743-8768. (9) Ribe N.M. (1988) *Earth Planet. Sci. Lett., 88*, 37-46. (10) Shearer C.K. and Papike J.J. Proc. (1989) *Lunar and Planet. Sci. Conf. 20th*, in press. (11) Lundberg L.L, Crozaz G., McKay G., and Zinner E. (1988) *Geochim. Cosmochim. Acta, 52*, 2147-2163. (12) Burghele A., Dreibus G., Palme H., Rammensee W., Spettel B., Weckwerth G., and Wanke H. (1983) *Lunar Planetary Science XIV*, 80-81. (13) McSween H.Y. and Jarosewich E. (1983) *Geochim. Cosmochim. Acta, 47*, 1501-1513. (14) Jones J.H. (1986) *Geochim. Cosmochim. Acta, 50*, 969-977. (15) Jagoutz, E. and Wänke, H. (1986) *Geochim. Cosmochim. Acta, 50*, 939-953. (16) Warren P. H. and Wasson J.T. (1979) *Rev. Geophys. Space Phys., 17*, 73-88.

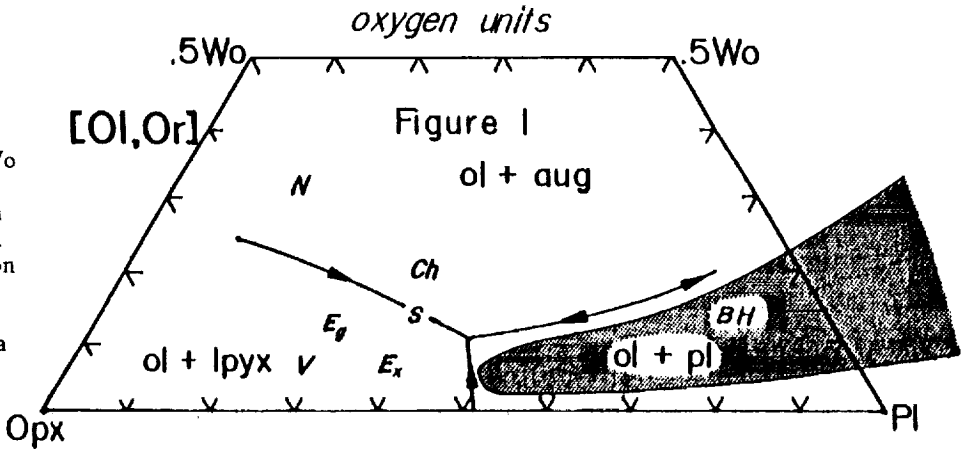

Figure 1. Compositions of SNC parent magmas projected onto Opx-Pl-Wo plane after (2). V is Viking soil composition (3); BH is 23 kb martian primary melt composition (4). Figure 2. Calculated REE in Nakhla and shergottite parent magma compositions.

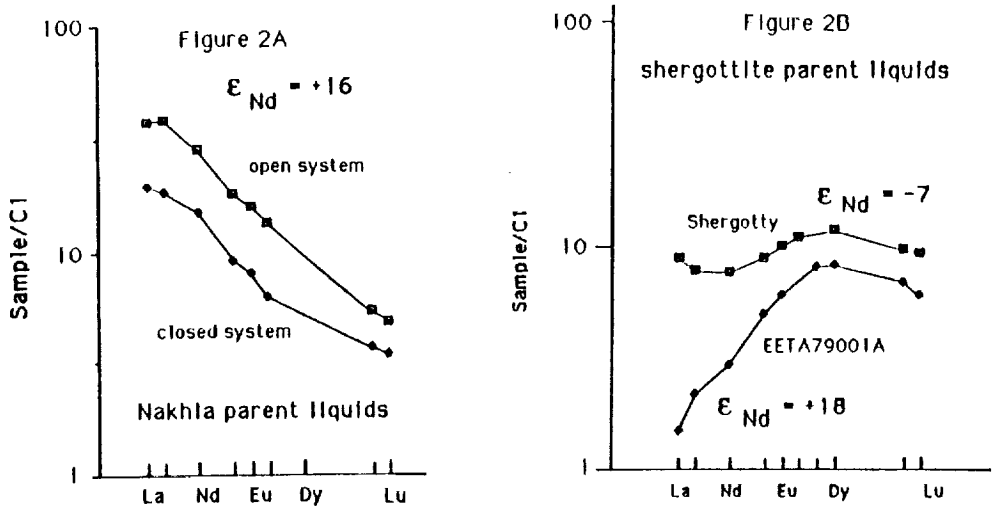

EMPLACEMENT AND GROWTH OF LAVA FLOW FIELDS ON EARTH AND MARS

Rosaly Lopes, Jet Propulsion Laboratory, Caltech, Pasadena, CA 91109
Christopher Kilburn, Osservatorio Vesuviano, 80123 Naples, Italy

The final morphologies of martian lava flow fields hold clues to their emplacement histories and can be used to infer effusive parameters, by using terrestrial lavas as analogues and presupposing similar emplacement regimes on Earth and Mars. Studies of terrestrial lavas suggest that the overall development of aa and blocky flow fields is systematic and may be characterised by the ratio of maximum width, Wm, to maximum length, Lm. Such systematic behaviour is interpreted in terms of the repeated generation of flows during the growth of a flow field, from which we have derived a general, normalised relation linking final dimensions (Wm, Lm, and average thickness) to the underlying slope and the total duration of the effusion. This relation (Fig. 1) is particularly useful for the study of extra-terrestrial lavas, since it links measurable morphological parameters to duration (and, therefore, average effusion rate and velocity), independent of any explicit knowledge of lava density, rheology, or gravitational acceleration. Using this relation, we obtained the durations, average effusion rates, and average velocities of 18 lavas on Alba Patera, which were selected on the basis of how well the relevant morphological parameters could be measured. To allow for errors in maximum length, we used a range of lengths for each lava, the minimum and maximum values corresponding to the traceable part of each flow field and to the greatest length obtained using inferred vent locations.

The durations obtained for Alba Patera lavas (Fig. 2) are comparable to those of similar terrestrial lavas. In contrast, the average effusion rates are significantly larger (about 10 to 100 times) than those typical for recent terrestrial effusions. However, the estimated sizes of feeding fissures and the lava volumes on Alba are also much larger than on Earth and, when we consider the average effusion rates per unit length of fissure, we obtain values which are comparable with those for recent terrestrial lavas (1 to 10 $m^2 s^{-1}$). The major differences between the martian and terrestrial systems thus appears to be related to rates of magma generation and storage before eruption.

In spite of the high effusion rates, the Alba Patera lavas appear to have had modest average velocities (about 0.01 to 7 m s^{-1}), which are comparable to those of terrestrial basalts. We used these velocities to investigate whether, given the dimensions of Alba's lavas, they are consistent with the laminar-crusted emplacement regime which is a requirement of our model. We found that laminar flow is ensured if: (1) lavas are more siliceous than basalt; (2) lavas are basaltic and had eruption temperatures below about 1140 ^{o}C (corresponding to crystallinities of about 30-40%); or (3) lavas are ultramafic (komatiitic) and had eruption temperatures of about 1250-1300 ^{o}C (i.e. crystallinities of about 50-60%). The first two conditions are perfectly reasonable by analogy with present-day Earth. However, if these Alba Patera lavas are komatiitic, applicability of our model would require conditions of magma ascent special to the martian environment.

Figure 1: Relation between flow field dimensions (maximum width, Wm; maximum length, Lm; and average thickness, h), underlying slope α and duration of eruption (T) for 123 lavas from Etna, Kilauea (including Pu'u O'o), Vesuvius, Arenal and 10 other volcanoes. The relation has the form:

$$T = (1/K)\ (Wm/Lm)\ h^2 \sin \alpha$$

where $K = 0.08\ m^2\ day^{-1}$ (range: 0.015 to 0.310 $m^2\ day^{-1}$) and is identified as lava thermal diffusivity.

FIG 1: TERRESTRIAL FLOW FIELDS

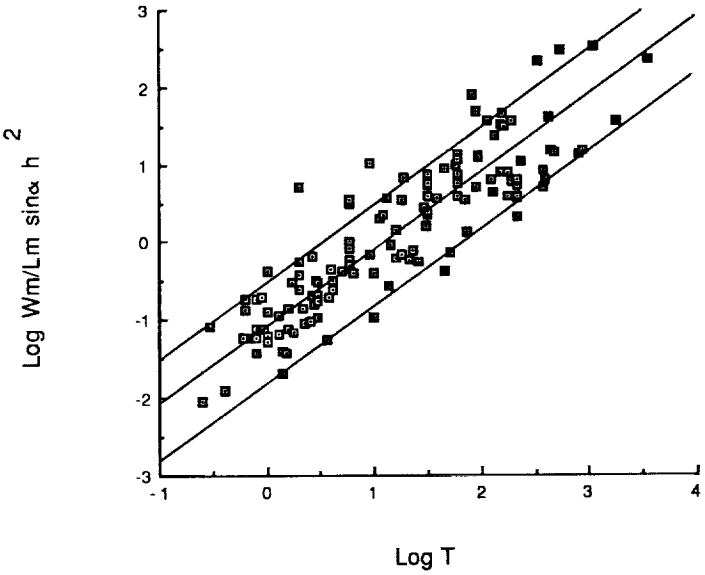

Figure 2: The relation shown in Figure 1 applied to Alba Patera lavas. the errors bars in (Wm/Lm) $h^2 \sin \alpha$ represent the range of lengths used for each flow field.

FIG 2: ALBA PATERA LAVAS

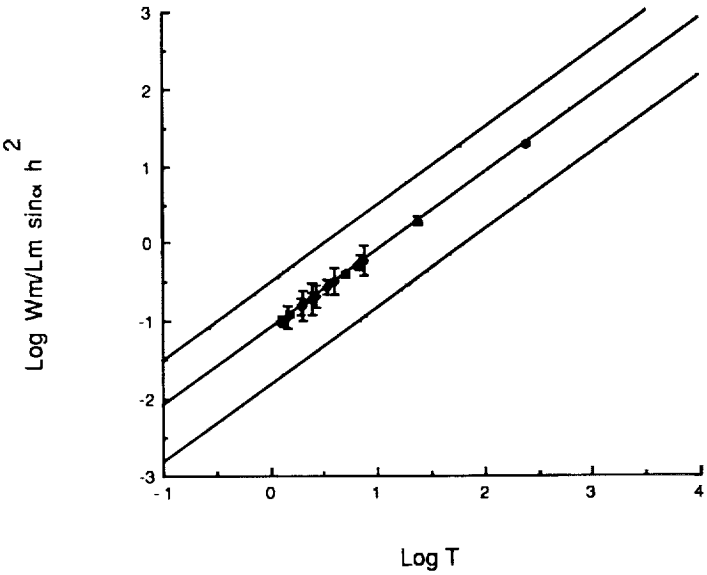

WHAT IF DEPOSITS IN THE VALLES MARINERIS ARE VOLCANIC?; Baerbel K. Lucchitta, U.S. Geological Survey, Flagstaff, Ariz. 86001

An intensive study of high-resolution stereoscopic images found that the deposits inside the Valles Marineris include two major types: an older layered sequence that forms high, eroded mesas approaching the elevation of the bounding plateaus [1,2] and a younger sequence composed of varied materials deposited on a deeply eroded surface whose elevation is close to that of the present trough floors. Both may be, at least partly, of volcanic origin.

The older layered deposits were emplaced during or shortly after erosion of the trough walls into spurs and gullies. They consist of dark and light layers. The dark layers are generally thin and some are resistant to erosion; the light layers are thick, poorly stratified, and highly susceptible to wind erosion. These layered deposits, because of their apparent horizontality and lateral continuity, may be lacustrine [3]. However, the volume of interior deposits is too large to have come solely from chemically precipitated [4], inflowing fluvial, or masswasted materials. The amount of eolian material that may have foundered through an ice cap on a lake [2] is probably also insufficient. The existence of resistant, thin, dark units, the susceptibility to deflation of thick, light units, and the volumetric insufficiencies of alternative processes support a volcanic origin for at least some of the layered deposits [5,6]; perhaps the even layering is due to eruption into a paleolake [2].

After the troughs had nearly reached their present configuration through late-stage faulting and erosion, new deposits of diverse morphology and albedo were emplaced [7]. These deposits are generally thin, but in western Candor Chasma they may reach thicknesses of 3 km. Light materials are locally massive bedded or wind fluted; some have lobate fronts. Dark deposits are spectrally nearly gray, have an albedo as low as 5 percent [8], and preferentially occur along fault lines. The younger deposits are not readily explained as lacustrine in origin, because they were emplaced late in Martian history when surface water was unstable in equatorial latitudes. They are too rugged and diverse to be solely eolian. Debris-flow origin is also unlikely because the deposits embay other masswasted features such as talus slopes on the walls of tributary canyons and landslides, and the deposits have no obvious source scars. A volcanic origin is consistent with the apparent flow lobes, the spectral signatures of the dark materials that suggest mafic compositions, the association of the dark materials with structures, and with deflation fluting similar to that seen on terrestrial tuffs in arid regions.

What are the implications if some of the interior deposits are indeed of volcanic origin?

(1) The Valles Marineris grabens would be more like terrestrial rifts that commonly contain volcanic rocks.

(2) Volcanism in this region of Mars would have taken place throughout the history of the Valles Marineris, extending from Early Hesperian to Late Amazonian and perhaps even to recent times.

(3) Early volcanism would have produced voluminous eruptions of flows and light-colored tuffs that formed evenly layered sheets over thousands of square kilometers. These deposits may have been subaqueous.

(4) Later, subaerial volcanism would have produced materials of diverse composition and morphology, including mafic pyroclastic and effusive products, and it would have emplaced voluminous ash-like deposits that flowed readily for tens of kilometers.

Questions arising from these implications include the following: (a) Can the even layering be explained by subaerial volcanism, or need subaqueous volcanism be invoked? If so, how would subaqueous volcanism function in the Martian environment? (b) If the light-colored deposits are indeed ash-flow tuffs, what is their composition? If they are silicic, the discovery would alter our perception of volcanism on Mars. (c) Can some of the ash production be explained by an unusually high volatile content of the magma or by interaction of the magma with the ice-rich regolith [9]?

Overall, the evidence points toward the presence of at least some volcanic rocks inside the Valles Marineris. If so, the timing of the eruptions, the composition of the rocks, and their emplacement mechanisms set important constraints on the magmatic evolution of Mars. The exploration of these possibly volcanic rocks should be a high priority on future missions to Mars.

References

[1] McCauley J.F. (1978) Geologic map of the Coprates quadrangle of Mars. U.S. Geological Survey Miscellaneous Investigations Series Map I-897, scale 1:5,00,000. [2] Nedell S.S., Squyres S.W., and Anderson D.W. (1987) Origin and evolution of the layered deposits in the Valles Marineris. Icarus 70, 409-441. [3] McCauley J.F., Carr M.H., Cutts, J.A., Hartmann W.K., Masursky Harold, Milton D.J., Sharp R.P., and Wilhelms D.E. (1972) Preliminary Mariner 9 report on the geology of Mars. Icarus 17, 289-327. [4] McKay C.P. and Nedell S.S. (1988) Are there carbonate deposits in Valles Marineris, Mars? Icarus 73, 142-148. [5] Peterson, Christine (1981) A secondary origin for the central plateau of Hebes Chasma. Lunar and Planetary Science Conference 12th, Proceedings, Geochimica et Cosmochimica Acta, 1459-1471. [6] Lucchitta B.K. (1987) History of Valles Marineris (abs.). In Lunar and Planetary Science 18, 572-573. [7] Lucchitta B.K. (1987) Recent mafic volcanism on Mars. Science 235, 565-567. [8] Geissler P.E., Singer R.B., and Lucchitta B.K. (1989) Valles Marineris: Compositional constraints from Viking multispectral images (abs.). In Fourth International Conference on Mars, (Tucson, Arizona: Jan. 10-13, 1989), 111-112. [9] Wilson L. and Head J.W. (1983) A comparison of volcanic eruption processes on Earth, Moon, Mars, and Venus. Nature 302, 663-669.

STATE OF STRESS AND ERUPTION CHARACTERISTICS OF MARTIAN VOLCANOES. Patrick J. McGovern and Sean C. Solomon, Department of Earth, Atmospheric, and Planetary Sciences, Massachusetts Institute of Technology, Cambridge, MA 02139.

Introduction. The growth of a large volcano exerts a load on a planetary lithosphere that can give rise to flexural deformation and faulting. Lithospheric stress, in turn, can influence the state of stress within the volcano and thus the characteristics of eruptions and the deformation and growth of the construct. Previous studies of the stress state within and beneath terrestrial volcanoes have been of two main types: (1) models of plate flexural stresses in isolation [1,2], or (2) finite element models of volcanic bodies with rigid lower boundary conditions [3,4]. We seek a model which couples the stress and displacement fields of both the plate and volcano structures, in order to understand the behavior of Martian volcanoes and the relationship of eruption styles to evolving local and regional stress.

Method. We use the finite element code TECTON, written by H.J. Melosh and A. Rafesky [5,6], to construct axisymmetric models of volcanoes resting on an elastic lithospheric plate overlying a viscoelastic asthenosphere. This code can model buoyancy forces supporting the plate, thus allowing a proper representation of plate flexure. Several values of the ratio of volcano size to lithospheric thickness were considered. The elastic plate was taken to have a thickness of 100 km, and the viscoelastic layer was taken to extend to a sufficient depth so that a rigid lower boundary has no significant influence on the results. The code first calculates elastic deformations and stresses and then determines the time-dependent viscous deformations and stresses. Time in the model scales as the Maxwell time in the asthenosphere.

Results. The deviatoric stress field (principal stress directions) resulting from the elastic deformation induced by a volcano 25 km in height and 775 km in diameter is shown in Fig. 1. Note that the principal stress directions on the surface layer of elements are rotated such that the most compressive stress direction is parallel to the topographic surface. The stress field after the plate has flexed under the volcanic load is shown in Fig. 2. We note two effects of plate flexure with increasing time: (1) the deviatoric stresses in the surface region grow quite large; and (2) the area where the principal compressive direction is parallel to the surface extends progressively deeper, eventually reaching into the crust beneath the construct. Also, at large times, the boundary between the area of rotated stress directions and the underlying area of 'normal' stress orientations (compression axis vertical) is a region of low deviatoric stress.

Discussion. The above effects of flexure on the volcano stress field may have important implications for the history of volcanic events. It has been suggested [1] that time-dependent flexural stresses at the top of the elastic lithosphere beneath the Hawaiian volcanic chain control the history of eruptions at individual volcanoes, with eruptions ceasing during intervals when the two principal horizontal stress deviators are compressive and of significant magnitude. Applied to our model, this would imply that at early times after an interval of significant shield-building eruptions, the horizontal stress deviators within and beneath the volcano are tensional, so magma ascent to high-level chambers within the construct is favored. At later times, the stress directions in and beneath the volcano rotate such that the most compressive axis is nearly horizontal, so high-level magma bodies and summit eruptions would not be expected unless the ascending magma is significantly overpressured. In contrast, given that magma propagates through conduits oriented perpendicular to the least compressive stress, the stress orientations shown in Fig. 2 imply that flank eruptions are preferred at this stage of development. The young ages of the volcanic units surrounding Olympus Mons and Tharsis Montes are consistent with such an evolution in eruptive style [7].

Conclusions. These initial models suggest that the state of stress during volcano growth and lithospheric flexure can have an important influence on volcano evolution on Mars. Further models are planned to examine the roles of magma chamber overpressure and evacuation and near-surface faulting on the stress orientations presented here.

References. [1] U. S. ten Brink and T. M. Brocher, *JGR, 92,* 13687, 1987; [2] C. H. Thurber and A. E. Gripp, *JGR, 93,* 4721, 1988; [3] L. Chevallier and W. J. Verwoerd, *JGR, 93,*

4182 1988; [4] J. H. Dieterich, *JGR, 93,* 4258, 1988; [5] H. J. Melosh and A. Rafesky, *GJRAS, 60,* 333, 1980; [6] H. J. Melosh and A. Rafesky, *JGR, 88,* 515, 1983; [7] D. H. Scott and K. L. Tanaka, *Icarus, 45,* 304, 1981.

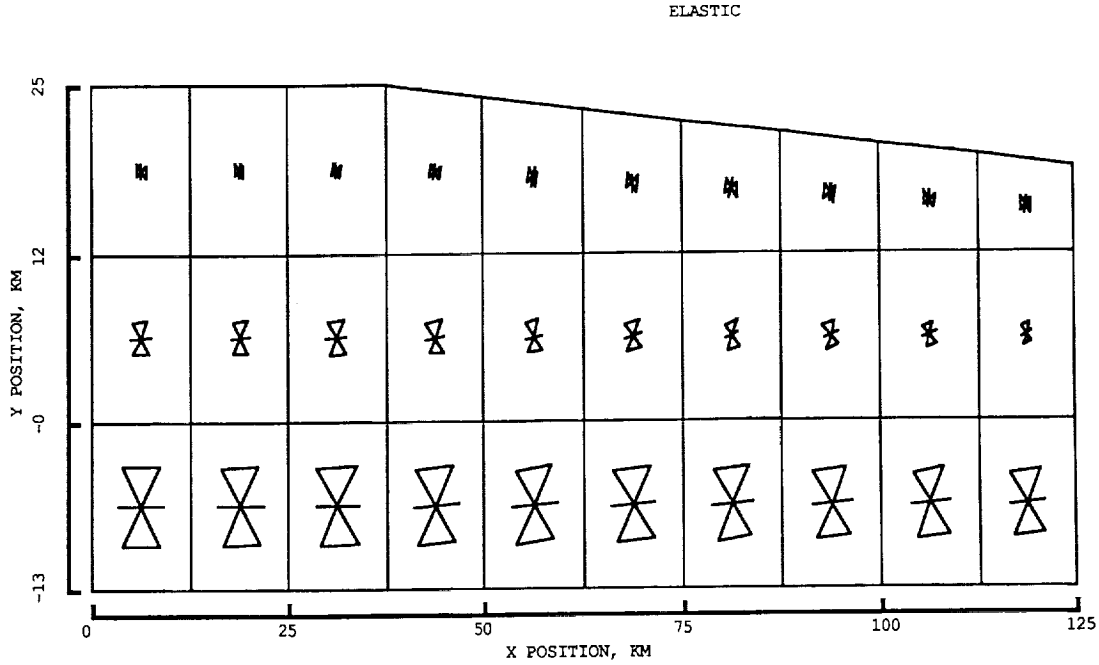

Figure 1. Close-up view of the deviatoric stress field in the volcano after the initial elastic deformation. An hourglass shape denotes the principal axis of compression, a bar denotes the principal axis of tension; the size of each symbol is proportional to deviatoric stress magnitude. The axis of rotational symmetry is x=0.

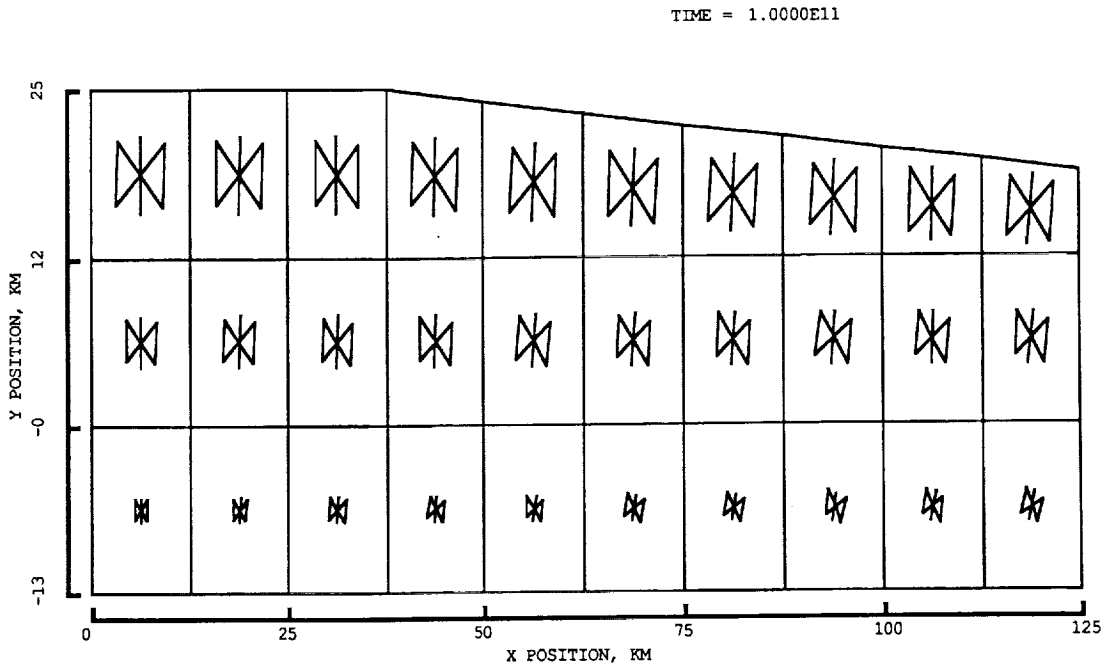

Figure 2. Deviatoric stress field in the volcano after flexure. The time elapsed is on the order of 100 Maxwell times. Rotation of the stress axes extends downward to the top layer of the plate (below y=0).

CO2 SOLUBILITY AND ITS IMPLICATIONS FOR DEGASSING ASCENDING MAGMAS;

Vivian Pan and John R. Holloway*, Dept. Geology, Arizona State Univ., Tempe, AZ 85287; *also Dept. of Chemistry.

INTRODUCTION Planetary degassing processes as well as rheologic properties of magmas are directly related to the volatile content of magmas. In order to address these topics we must know the solubility of the dominant volatile components in relevant magmatic liquids at the appropriate pressures and temperatures. The present day Martian atmosphere indicates that carbon is an abundant component on the planet. Additionally, SNC meteorites record magmatic oxygen fugacities (fO_2) near that of the quartz-fayalite-magnetite (QFM) buffer [1]. Thus at QFM, carbon that is involved in melting events is in the form of CO_2 [2]. This experimental study was initiated to determine the solubility of CO_2 in relevant Martian magma compositions. The results to date have been obtained on a mafic composition at 10, 15 and 20 kb total pressure. We also compare solubility models for terrestrial tholeiites and for the Martian model composition.

CHOICE OF COMPOSITION CO_2 solubility is compositionally dependent [3,4], therefore, we must select for our experiments compositions that are representative of Martian magmas. Unfortunately, Martian magma compositions are not directly known so we must rely on other methods to surmise their composition. Inferences from SNC meteorites suggest that their parental magmas are of a low-Al, mafic to ultramafic, silica-saturated composition similar to terrestrial basaltic komatiites except for higher Fe/Mg (summarzied by [5]). In addition, preliminary data from melting experiments on the Dreibus & Wänke bulk mantle composition [6] agree favorably with the estimated SNC parental magma compositions as probable volcanic compositions on Mars [7]. We have chosen the parental composition of EETA79001 lithology B (groundmass texture; representing liquid), **Eg**, estimated by [5] as the relevant composition for this study (Table 1). This composition differs significantly in Fe/Mg ratio from previous determinations on mafic terrestrial compositions. We also performed a few experiments on a 1921 Kilauean olivine tholeiite to test the solubility model of [8].

EXPERIMENTAL TECHNIQUES AND ANALYSIS Experiments were performed in a non-end-loaded piston cylinder apparatus with a 0.5" diameter solid-media pyrex-NaCl assembly. The starting material was synthesized from reagent grade oxides in a gas mixing furnace at fO_2 of one $\log_{10}$ unit lower than QFM. The Pt capsules used were pre-saturated with Fe to minimize Fe loss. Silver oxalate was used as the CO_2 source. Run temperatures were 1400-1500°C and run durations ranged from 0.5 to 2 hrs. Quantitative and speciation analyses of carbon in the glass run products were performed with a fourier transform micro-infrared spectrometer. We utilized the extinction coefficients for OH^- and CO_3^{2-} from [9,10]. In addition, thermal gravimetric analyses were performed on two samples to corroborate the IR analysis.

RESULTS The experimental results are listed in Table 2. The IR spectra of the run products show that CO_3^{2-} is the only carbon species dissolved in the glasses. The positions of the CO_3^{2-} ν 3 antisymmetric stretch bands are located at 1515 cm^{-1} and 1415 cm^{-1} similar to the location for MORBs determined by [9]. All samples contained ~ 0.1wt% H_2O as determined by the small peak located at 3527 cm^{-1} representing the strecthing of OH^- groups.

Our solubility results for the 1921 Kilauean olivine tholeiite composition agree very well with the concentration predicted by the model of [8] (Figure 1). We now have demonstrated the positive temperature dependence of solubility, and that $\Delta H°$ of 21.5 kcal/mole is a reasonable value for tholeiites. The experimental results of the Martian model composition Eg do not, however, show as great a temperature dependence as the tholeiite. Assuming that $\ln K(P_O,T_O)$

and $\Delta V_r°$ for Eg are near the values for tholeiite (-15.15±.06 and 33 cm^3/mole, respectively), we calculate a $\Delta H°$ of 18.10 kcal/mole. Figure 2 displays the solubility model predicted for Martian composition Eg.

Under the conditions examined thus far, the solubility of CO_2 in the model Martian melt composition is very low and lower than the solubility in terrestrial tholeiites. Our solubility model implies that at low pressures, the density and perhaps the viscosity of the model Martian magma are not significantly changed in the situation of CO_2 saturation. Furthermore, if glass inclusions exist within the SNC meterorites we may be able to utilize this solubility model to investigate the degassing history of the magma bodies, provided that there was sufficient carbon in the Martian mantle to yield CO_2 saturation.

REFERENCES [1] Stolper, E. and McSween, H.Y., Jr., 1979, Geochim.Cosmo.Acta., V.43, 1475-1498.[2] Eggler, D.H., 1978, Am. J. Sci., V.278, 305-343.[3]Mysen et al., 1975, Contrib. Min. and Pet., V.53, 227-239.[4] Brey, G. and Green, D.H., 1975, Contrib. Min. and Pet., V.49, 93-103.[5] Longhi, J. and Pan, V., 1989, Proc. 19th Lunar and Planet. Sci. Conf., 451-464.[6] Dreibus, G. and Wänke, H., 1984, Proc. 27th Intern.Geol. Cong., V.11, 1-20.[7] Bertka, et al., 1990, this volume. [8] Stolper, E. and Holloway, J.R., 1988, EPSL, V. 87, 397-408. [9] Fine, G. and Stolper, E., 1986, Earth & Planet. Sci. Lett., V.76, 263-278.[10] Newman et al., 1986, Am. Min., V. 71, 1527-1541.

Table 1.
Martian Model Composition Eg [5]

SiO2	TiO2	Al2O3	FeO	MgO	CaO	Na2O	Total	Mg#
50.67	0.86	7.10	18.67	12.22	8.74	1.07	99.33	0.54

Table 2. Results of solubility experiments for model Martian composition (Eg) and olivine tholeiite (1921K).

	Eg1	Eg6	Eg4	Eg13	1921K-4	1921K-1	1921K-2
P(kb)	10	10	15	15	10	15	15
T(°C)	1400	1400	1450	1500	1400	1400	1500
CO2(wt%)	0.65±.10	0.61±.09	0.94±.14	1.11±.17	0.73±.11	0.96±.14	1.37±.21
H2O(wt%)	0.14±.02	0.08±.01	0.09±.01	0.09±.01	0.036±.006	0.030±.005	0.044±.007
X(CO2)^	0.66	0.76	0.8	0.84	0.89	0.93	0.93
ΔH°(calc)	19.28±.52	17.71±.52	17.54±.52	17.86±.52	22.16±.52	21.90±.52	21.59±.52

^ mole fraction CO2/(CO2+H2O)

Fig 1. CO2 solubility model for tholeiite [8]

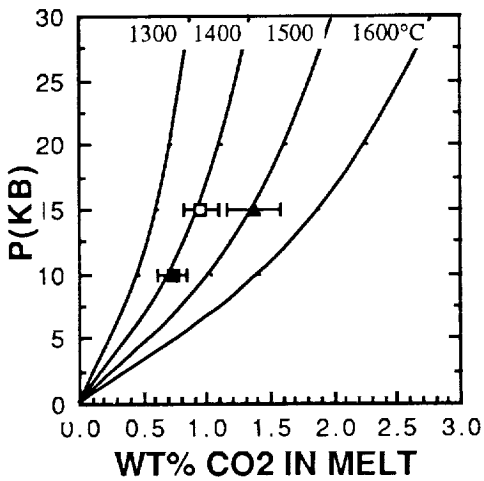

Fig 2.CO2 solubility model for composition Eg

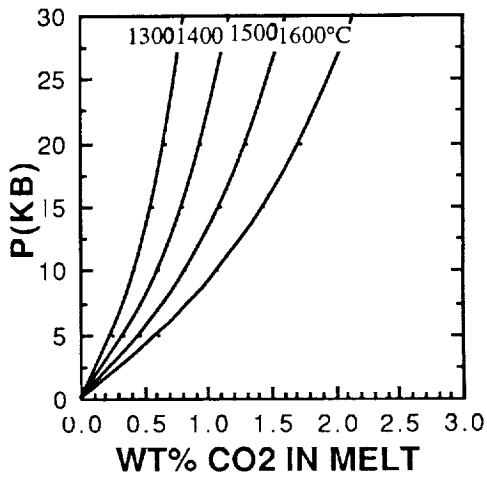

WATER AND EVOLVING MAGMA BODIES ON MARS; Cordula Robinson ULO Planetary Image Centre, 33-35 Daws Lane, London, NW7 4SD.

Discovery of apparent fluvial features on Mars has resulted in continued discussion about the source of the water and the processes that enable its intermittent generation on the surface throughout the planet's history (1, 2, 3, 4, 5). Evidence based on stratigraphy, spatial distribution of channels, and water budget, indicate that the release of water can be explained by volcanic thermal activity.

The unconfined outflow channels can be directly related to a source of increased thermal activity, ie. they are peripheral to the Tharsis Province, and are penecontemporaneous with the plains forming Chryse Planitia (2, 6). It is proposed that the water has a juvenile origin. It was released from a fractionating magma body, and became trapped as ice in the overlying mega-regolith. Subsequent high level magmatism led to the release of water at the surface. This type of mechanism can be applied to the Elysium region where confined outflow channels are also concentrated around an area of pronounced volcanism (7).

The origin of water carving the runoff channels remains ambiguous. The channels are not tied to a fixed source of volcanism but are pervasive (6, 7). One of three alternatives, related to volcanic thermal activity, may apply to their development. This would remove the need for a radical change in the martian climate - an issue also emphasised by Gulick and Baker (8, 9):

1. As for the outflow channels, but from a magma source leading to plateau type volcanism rather than central vent volcanism.
2. As for 1. but water was then recycled back into the mega-regolith to be re-released with continued volcanism.
   or
3. Stemming from primordial outgassing and being retained globally in the mega-regolith as ice. An increase in thermal gradient associated with plateau volcanism, melted the ice and provided the water to carve the features.

The interpretation of fluvial features in this manner is important in two essential ways. Firstly, the volume of water anticipated to have outgassed, based on geomorphological observation (1), is reduced to be more in accordance with geochemical models (1). The requirement, therefore, that 350m. of unbound water needs to be stored planetwide in the mega-regolith for outflow channel formation is removed. Secondly, the observations suggest that the generation and liberation of surface water is genetically connected to "evolving magma bodies".

WATER AND EVOLVING MAGMA BODIES ON MARS; Cordula Robinson.

References:

(1) MH Carr (1986) Icarus 68 p.187-216.
(2) MH Carr (1981) Surface of Mars.
(3) MH Carr, GD Clow (1981) Icarus 48 p.91-117.
(4) DE Wilhelms, RJ Baldwin (1989) Proc.LPSC 19 p.355-365.
(5) SW Squyres, MH Carr (1986) Sci 231 p.249-252.
(6) DH Scott, KL Tanaka (1986) USGS Map-I-1802-A.
(7) R Greeley, JE Guest (1987) USGS Map-I-1802-B.
(8) VC Gulick, VR Baker (1989) Nature 341 p.514-516.
(9) VC Gulick, MS Marley, VR Baker (1988) LPSC 19 p.441-442.

CONTAMINATION OF THE MARTIAN MANTLE BY BASIN-FORMING IMPACTORS; P.H. Schultz and R.W. Wichman, Brown University, Providence, R.I. 02912.

Introduction: The record of major impact basins on Mars is partly hidden both by a period of intense gradational activity early in its history and by subsequent volcanism (1, 2). Hellas, Chryse, Isidis, and Argyre impact basins nevertheless establish that Mars was impacted by asteroid-size objects (300-600 km in diameter) at a time when the lithosphere may have been only 100 km thick (3, 4, 5). Although impact velocities at this time are poorly constrained, large co-orbiting objects arriving from the asteroid belt not only seem dynamically possible but could be indicated in the central peak/ring morphology of smaller craters and basins (6). This paper explores the possible role of such low-velocity impacts for locally contaminating the martian mantle (impactor and down-driven crustal materials) and for contributing to observed trends and contrasts in the volcanic evolution of impact basins across Mars.

Sequence of Basin-Related Volcanism: Numerous studies have described the general sequence of martian volcanism: from the ancient upland intercrater plains (7); to possible early silicic-like construction (8); to the distinctive and eroded highland patera (9, 10) contemporary with the vast mare-like ridged plains; and finally the major volcanic domes, tholi, and shields (9). The early volcanic history on Mars, however, can be linked to tectonic patterns associated with the major impact basins (5, 11). A common volcanic and tectonic chronology emerges for the Isidis and Hellas basins. Radial and concentric zones of lithospheric failure develop soon after basin formation, most likely due to the response of the thin lithosphere to the basin transient cavity. Although impact-triggered, mare-like volcanism may have extensively resurfaced the basin interior and periphery, thick friable deposits and other sediments largely mask the details of this history. Hadriaca and Tyrrhena paterae occur along a structural trough extending radially from Hellas and appear to represent a more volatile-rich style of early volcanism. Vast mare-like ridged plains inundate peripheral basin lows, but more significantly, large constructional shields develop to one side on the massif rings of both Hellas and Isidis. This phase of shield construction dominates the last stages of volcanic activity.

Thus, the volcanic history of Isidis and Hellas seems to evolve from volatile-rich to volatile-poor styles culminating in offset shield construction. In addition, thick deposits of easily eroded material become trapped within the interior of Hellas and may reflect products of early volcanic styles as well as long-term accumulations of trapped sediments. The evolving volcanic styles reflect in part the interplay of volcanism and a volatile-rich crust recycled (exposed, buried, re-distributed) during the formation of major impact basins (2). The hypothesis proposed here extends this recycling process by directly injecting volatile-rich contaminants into an evolving martian mantle.

Low-Velocity Basin Impactors: Numerous experimental and theoretical studies have detailed the effect of vertical impacts on the displacement of target material and the fate of the impactor. At low impact velocities (<7 km/s), one dimensional calculations reveal that the projectile shock reaches its trailing surface before significant penetration of the target. Internal energy losses in the projectile include mechanical failure and perhaps shear heating, with only marginal shock heating due to the low impact velocity. As a result, a significant fraction of the projectile is driven downwards and lines the growing transient cavity while compressing and burying the largely intact stratigraphy of the pre-impact crust. This process is clearly shown in experiments (12, 13) and in numerical codes (14) for 5 km/s impact velocities. The terrestrial cratering record also reveals down-driven crustal sections (with subsequent uplift) but the characteristic impact velocities (typically exceeding 15 km/s) preclude projectile survival *en masse* as violent decompression and shock vapor pressures disperse this signature. For very low velocity impacts on Mars, greater fractions of the projectile accompany the downdriven crust.

Most impacts, however, do not occur vertically. Gault and Wedekind (15) documented the systematic change in crater shape (profile and plan) as a function of impact angle. More recently, Schultz and Gault (16) explored both the contrast in energy partitioning and the fate of the projectile

MANTLE CONTAMINATION
P.H. Schultz and R.W. Wichman

as a function of impact angle. Vertical impactors may survive on the floor of final crater in porous and non-porous targets, whereas oblique impactors invariably ricochet out of the cavity due to upward-directed shock and spallation. Moreover, the penetration depth of the projectile and the downward-displaced target sections decrease significantly with impact angle.

At basin-scales, these basic processes should apply, but fundamental differences also may emerge. For example, most existing scaling relations between displaced mass and independent impactor variables (17) predict that a 6 km/s impact by a 400 km-diameter asteroid on Mars should produce a transient cavity about only slightly larger than its diameter. This paradox partly reflects the effect of extreme extrapolations. It also may reflect a fundamental change in crater shape at large scales where the zone of maximum projectile penetration and downward displacement is surrounded by a shallower zone of gravity-controlled transient crater growth (6). The degree of penetration, however, still depends on impact angle.

These idealized starting conditions permit framing a conceptual model for the possible consequences of late-stage, basin-forming impactors (300-600 km) on a thermally evolving Mars. At low impact velocities, near-vertical impacts should significantly contaminate the upper mantle and asthenosphere with both meteoritic and crustal materials as the projectile penetrates well below the 100 km-thick lithosphere. As penetration times exceed times required for viscous creep, subduction of crustal materials and engulfment of the projectile may be possible (18). Oblique impacts ($\preceq$ 45°), however, result in significantly less contamination as the impactor fails, shears, and spalls prior to penetrating a distance equal to its radius into the planet. Consequently oblique impacts should contribute a veneer of reworked crustal material mixed with dispersed impactor debris. The importance of mantle contamination and its possible effects, then, hinges on occurrence of the very rare but probable near-vertical (<70°) impacts.

While very low angle impacts at smaller scales create a distinctive geomorphic signature, near-vertical impacts at basin scales may create a distinctive sequence of volcanic styles with early volatile-contaminated mantle materials evolving to more mafic effusions. Just as a rare "grazing" basin impact may create a catastrophic effect on the martian climate, a rare near-vertical impact may initiate a unique response of the interior recorded in the geologic record. Impactor and crust materials injected into the mantle could lead to basin-localized continental style volcanism and degassing, extended thermal lifetimes due to the concentration and burial of radiogenic nucleides, and a progression of volcanic styles.

References: (1) Schultz, P.H., Schultz, R.A., and Rogers, J. (1982) *J. Geophys. Res., 87,* 9803-9820. (2) Schultz, P.H. (1988) *MEVTV Workshop on the Nature and Composition of the Cratererd Uplands on Mars,* Tech. Rept. 88-05, 117-119, LPI. (3) Schubert, G., Cassen, P. and Young, R.E. (1979) *Icarus, 38,* 192-211. (4) Solomon, S.C. and Head, J.W. (1982) *J. Geophys. Res., 87,* 9755-9774. (5) Wichman, R. and Schultz, P.H. (1989) *J. Geophys. Res.* (in press). (6) Schultz, P.H. (1988) In *Mercury* (F. Vilas *et al.*, eds.), U. Arizona Press, 274-335. (7) Greeley, R. and Spudis, P.D. (1981) *Rev. Geophys. Space Phys., 19,* 13-41. (8) Scott, D.H. (1982) *J. Geophys. Res., 87,* 9839-9851. (9) Plescia, J.B. and Saunders, R.S. (1979) *Proc. Lunar Planet. Sci. 10th,* 2841-2859. (10) Carr, M.H. (1981) *The Surface of Mars,* Yale Univ. Press, 232 p. (11) Schultz, P.H. (1984) *Lunar and Planet. Sci. 15,* 728-729. (12) Gault *et al.* (1968) In *Shock Metamorphism of Natural Materials,* 87-100, Baltimore, Mono. (13) Stoffler, D., Gault, D.E., Wedekind, J. and Polkowski, G. (1975) *J. Geophys. Res., 80,* 4062-4077. (14) Orphal, D.L. *et al.* (1980) *Proc. Lunar Planet. Sci. Conf. 11th,* 2309-2323. (15) Gault, D.E. and Wedekind, J.A. (1978) *Proc. Lunar and Planet. Sci. Conf. 9th,* 3843-3825. (16) Schultz, P.H. and Gault, D.E. (1989) *Proc. Conf. on Global Catastrophes in Earth History* (in press). (17) Schmidt, R.W. and Holsapple, K. (1982) In *Geol. Sco. Am. Sp. Paper 190* (L. Silver and P. Schultz, eds.), 93-102. (18) Wichman, R. and Schultz, P.H. (1989b) This volume.

TECTONIC SETTING OF MARTIAN VOLCANOES AND DEEP-SEATED INTRUSIVES

D.H. Scott and J.M. Dohm, U.S. Geological Survey, Flagstaff, AZ 86001

More than 50 volcanoes have been mapped on Mars [1,2,3], and recent geologic studies [4] indicate structural evidence of deep-seated intrusive bodies (Fig. 1). Most volcanoes in the Tharsis region are volcanotectonic features: they have been associated with large-scale tectonic and volcanic processes. They occur along complex systems of faults and grabens having a dominant northeast-southwest trend closely coincident with a great circle [5], which extends along 90° of arc from Tempe Patera to probable volcanic mountains near lat 40° S., long 150°. Olympus Mons, Alba Patera, and a small volcano between them are aligned nearly parallel to the Tharsis axial trend; the boundary of the Martian crustal dichotomy is largely covered by young lava flows in this region but appears to lie within the corridor between these two trends. Clusters of relatively small volcanoes occur around the south end of the Tharsis rise, particularly in the Thaumasia area where ancient rocks are transected by networks of intersecting faults.

Deep-seated intrusive bodies are also concentrated in the Tharsis region and are recognized mostly where faults have been deflected around their cores. The intrusives have no observable topographic expression or associated lava flows except for Tempe Patera [6], a relatively small volcano that appears to be the surface expression of a much broader and older intrusive body. Three large, circular, rimless structures clustered in the southwestern part of the Tharsis region (Fig. 1) do not resemble impact craters and may be volcanotectonic depressions [7].

The Elysium Mons-Amphitrites Patera volcanic alignment is subparallel to that of Tharsis but is longer, extending through about 120° of arc; it transects the dichotomy boundary and is radial to the Hellas basin. Unlike the Tharsis trend, however, it is not associated with recognizable fault or graben systems. No evidence of intrusive bodies has been found along this trend or in the entire eastern region of Mars. Several volcanoes occur in the south polar region [3] but here, too, no major fault trends or intrusives are present. Many small volcanoes and pyroclastic cones occur in the northern lowland plains, but even medium-size (≈50-km-diameter) volcanotectonic structures are not discernible; if they exist, lava flows of Late Hesperian and Amazonian age have probably obscured all evidence of their presence.

Volcanoes in the Tharsis region have the widest age range (Early Noachian-Late Amazonian) of all volcanoes on Mars, as determined by the size-frequency distribution of their craters having diameters of 2, 5, and 16 km. Volcanotectonic intrusive centers in the Tempe area are Middle Noachian to Late Hesperian, as indicated by faults of these ages that have been partly deflected around their centers. Volcanoes in the eastern hemisphere are Hesperian to Early Amazonian.

References

[1] Scott D.H. and Tanaka K.L. (1986) U.S. Geol. Misc. Inv. Ser. Map I-1802A. [2] Greeley R. and Guest J.E. (1987) U.S. Geol. Survey Misc. Inv. Ser. Map I-1802B. [3] Tanaka K.L. and Scott D.H. (1987) U.S. Geol. Survey. Misc. Inv. Ser. Map I-1802C. [4] Scott D.H. and Dohm J.M. (in press) Lunar and Planet. Sci. Conf. 20. [5] Wise D.U., Golombek M.P., and McGill, G.E. (1979) Icarus, 38, p. 456-472. [6] Plescia J.B. and Saunders R.S. (1979) Proc. Lunar Planet. Sci. Conf. 10, p. 2841-2859. [7] Scott D.H. (1982) Jour. Geophys. Res., 87, p. 9839-9851.

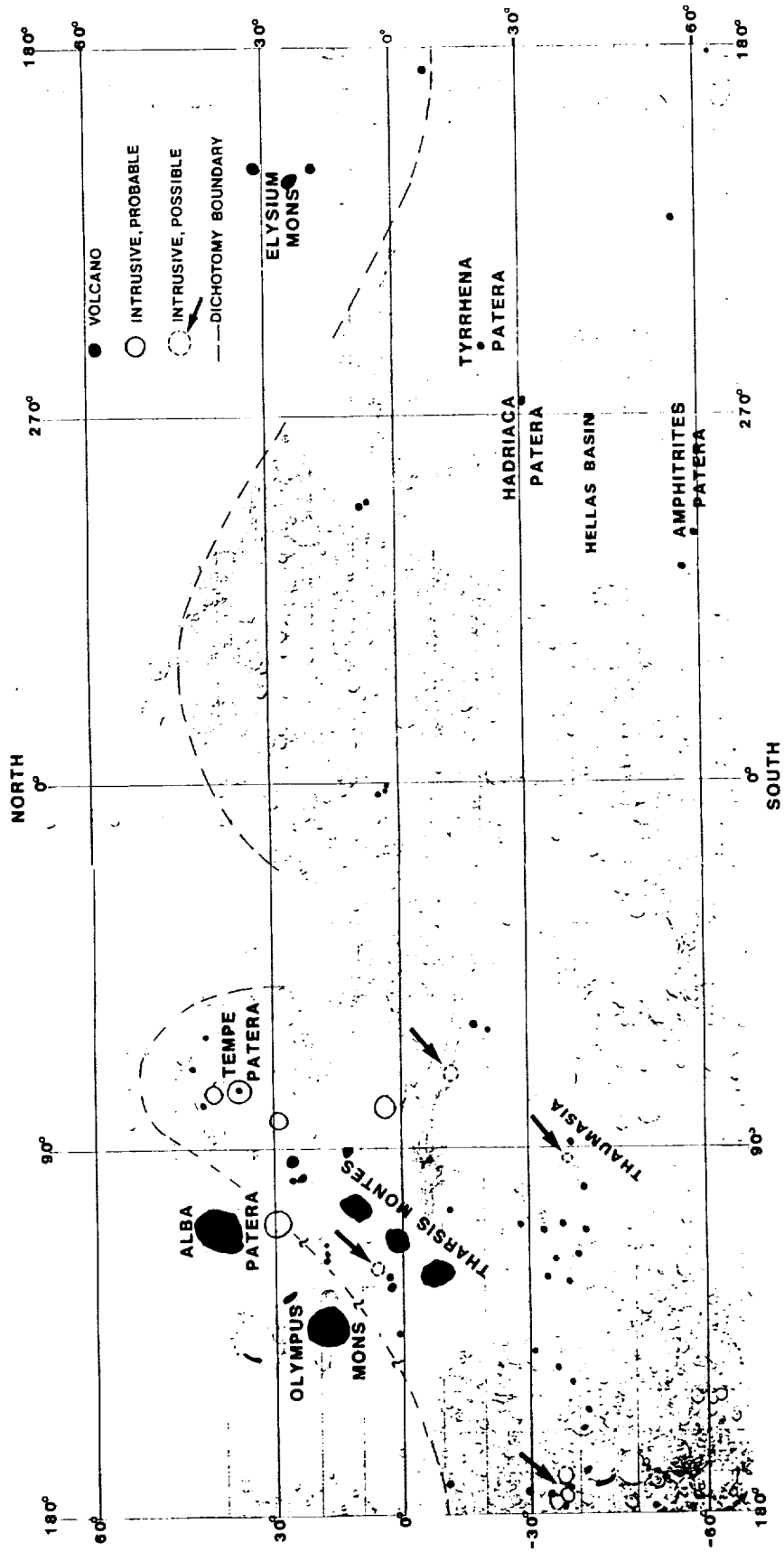

FIGURE 1

VOLCANOTECTONIC FEATURES ON MARS

RHEOLOGICAL PROPERTIES OF MARTIAN MAGMAS: EXPERIMENTS AND INFERENCES; F. J. Spera, and D. J. Stein, Both at Department of Geological Sciences and Institute for Crustal Studies, University of California, Santa Barbara, California 93106

Virtually every magma transport process of relevance to planetary magmatism and volcanism involves the diffusion of momentum. The rheological properties of both melts (single phase) and magmatic multiphase mixtures (melt plus crystals, melt plus vapor, etc.) are consequently of primary importance when evaluating the thermal history and volcanic evolution of a planetary body. Dynamic processes such as the extraction of melt from a source region, the propagation and ascent of melt or magma filled cracks, the convective dynamics of magma bodies, and the eruption of magma upon the surface of a planet cannot be quantitatively addressed unless accurate constitutive relations which properly account for the variation of rheological parameters with temperature, pressure, bulk composition, oxygen fugacity, the volume fraction and size and shape characteristics of suspended crystals and vapor bubbles are available. An approach based on both theory and experiment has proven to be most fruitful in the search for generally applicable models. Experimental concentric cylinder viscometry on a model Martian mafic magma (MMM) of shergottitic bulk composition (~50% SiO_2, 20% FeO_t, 10% MgO) at a range of hyperliquidus to near liquidus temperatures and fo_2's along QFM indicate that MMM behaves as a Newtonian fluid in the shear rate range 0.5 to 10 s^{-1}. The viscosity-temperature dependence is Arrhenian with activation energies in the range 170 to 220 kJ/mol. Absolute viscosities along QFM are rather low reflecting the high proportion of network modifying cations (high NBO/T ratios). Along QFM at 1250 < T < 1350°C, the ratio $X_{Fe_2O_3}/X_{FeO}$ where X_i is the mol fraction of the i^{th} component in the melt is around 0.08 and typical viscosities lie in the range 1 to 20 Pa s (10 to 200 poise). In the more oxidizing environment of the present day Martian atmosphere, log fo_2 at 1500 K is approximately -4.8; this leads to a predicted ratio of $X_{Fe_2O_3}/X_{FeO}$ of about 0.44 (1) in MMM. Because Fe^{3+} is at least partially located in network-forming tetrahedral sites, shear viscosities are expected to be perhaps as much as an order of magnitude larger than in QFM buffered melts assuming equilibrium with ambient Mars atmosphere at high temperatures. In other concentric cylinder experiments, the rheometric properties of solid plus melt and melt plus vapor magmatic mixtures have been studied. It is important to note that multiphase suspensions (s + m) and emulsions (m + v) are much more difficult to characterize compared to melts because of particle-particle or bubble-bubble interactions. These effects render the rheological properties highly non-linear. At low rates of strain (10^{-2} s), the viscosity of solid-melt suspensions is given approximately by $\eta = \eta_m [1 - \phi/A]^{-2}$ where ϕ is the volume fraction solids and A is a constant which depends on the size and shape distributions of the crystals. The Maron expression works best for melt viscosities > 10^2 Pa s because of the relative unimportance of particle-particle interactions. At higher shear rates when $\eta_m < 10^2$ Pa s, suspensions undergo shear thinning. A power law model of the form $\tau = m\gamma^n$ where n, the stress index, is inversely proportional to ϕ seems to fit data as well as the oft-quoted Bingham model. A Hawaiian basalt at 1120, 1110 and 1100°C gives ϕ = 0.27, 0.31 and 0.35 approximately with clinopyroxene, plagioclase and Fe-Ti oxides as phenocrysts. Measured yield

Rheological Properties of Martian Magmas
F. J. Spera and D. J. Stein

stresses (τ_o) and plastic viscosities η_p for the Bingham model are: (1.92 ± .4 x 10^4 N/m^2, 6.6 ± 1.7 x 10^3 Pa s), (3.5 ± .5 x 10^4 N/m^2, 5.5 ± 1.5 x 10^3 Pa s) and (4.5 ± .2 x 10^4 N/m^2, 1.7 ± .5 x 10^3 Pa s) respectively for the three temperatures. Alternatively, the power-law fit gives for m and n: (2.9×10^4 Pa s^{n-1}, 0.36), (4.2×10^4 Pa s^{n-1}, 0.27) and (4.6×10^4 Pa s^{n-1}, .13) for the same samples at 1120, 1110 and 1100°C, respectively. Note the correlation of τ_o on n, the power-law index with the volume fraction solids (ϕ). Large scatter is due, not to problems with instrumentation, but rather to the complex nature of flow within the region undergoing shear because of the presence of suspended phenocrysts of variable size and shape and perhaps local variations in their concentration. At very high shear rates for high volume fraction solid suspensions, experiments suggest dilatant behavior (shear thickening) due to the formation of structures within the mixture. Some data on a crystal rich magma from the 1983 eruption of Mt. Etna with about $\phi \simeq 0.40$ suggest dilatant power-law indexes around 1.5. For such shear thickening suspensions, brittle failure often occurs as shear rates are increased. Preliminary results for dilute melt plus vapor emulsions indicate that even a small fraction of vapor imparts viscoelastic properties to the mixture. Both shear thinning and shear thickening behavior has been noted. Application of results to melt segregation within the Martian mantle suggests a rather small compaction length scale O (10^2 m), high crystal-melt separation velocities O (0.1 m/yr) and consequently a relatively short time scale O (10^4 to 10^5 yr) for separation of melt from the source region. Based on estimated NBO/T ratios for analog Martian mafic melts, pressure has relatively little influence on melt viscosity. Magma driven fracture must be the mechanism for transport of magma through the Martian mantle-crust system as on Earth to avoid heat death.

The results of some ballistic models for the growth of Martian cinder cones taking account of the Reynolds number - drag coefficient relationship determined by wind tunnel experiments enable one to make definite predictions regarding Martian cinder cones that may be checked against Mars Observer data. (1) Kilinc, A., Carmichael, I. S., Rivers, M. L., Sack, R. O. (1983), Contrib. Mineral. Petrol., v. 83, p. 136-140.

A MODEL OF CRUSTAL SUBDUCTION BY LARGE IMPACTS AND THE IMPLICATIONS FOR SUBSEQENT MANTLE EVOLUTION; R. W. Wichman and P. H. Schultz, Dept of Geological Sciences, Brown University, Providence, R.I. 02912.

Introduction: In the standard model of crater excavation, the transient cavity develops from a combination of ballistically ejected material and downwardly displaced, shock-compressed material with a total ejecta volume of approximately half the final transient cavity (e.g., 1, 2, 3, 4, 5). In large craters, this transient cavity collapses to the final crater form with uplift and inward flow of the shocked, displaced material comprising the crater floor (6). This idealized model of crater formation fits many of the observed well-preserved planetary impact structures but it implictly assumes an elastic halfspace beneath the target surface which may be inappropriate for early, large, basin-forming impacts. For these very large impacts, the depth of the transient cavity may excede the lithospheric thickness and, at least on Mars, such cavities apparently can interact with an underlying viscous mantle regime during basin formation (7). Further, the extreme size of these cratering events also may negate some of the assumptions concerning cavity growth and collapse derived from smaller structures (8). In this abstract, we propose that viscous deformation at depth can allow emplacement of vertically displaced crustal material in the mantle, and we speculate on the implications such "impact subduction" might have on subsequent mantle evolution and partial melt compositions.

Subduction Model: Although material flow fields during crater excavation induce ballistic trajectories in most near-surface regions of the transient cavity, the target volume immediately beneath the impactor cannot achieve such trajectories. Consequently, a full target section is preserved at the center of the impact. In the case of an elastic half space, compression of this section against undeformed rocks at greater depth enhances lateral flow, disrupting the column and spreading it across the base of the transient cavity. If viscous flow occurs beneath the impact, however, downward displacement of this crustal section is partly accomodated by lateral flow in the mantle below. This process transfers impact deformation from the crustal section to the mantle and results in the emplacement of shocked crustal material into rocks of the upper mantle or asthenosphere. Later dynamic rebound might limit the depths such material could reach, but probably would not completely reverse burial since rebound affects the region beneath the crater as a whole and not the displaced elements of the transient cavity alone.

The key assumption for this impact subduction model is that the mantle acts viscously during the impact. This can be evaluated by comparing the Maxwell time (T_m) of the mantle to the duration of the impact event, where $T_m = \tau/2\mu\,\dot{\epsilon}$ and τ is applied shear stress, μ is shear modulus (~ 10^6 MPa) and $\dot{\epsilon}$ is strain rate of deformation.The Maxwell time is defined as the time required for viscous creep under stress to equal elastic strain (9); consequently, viscous behavior occurs when deformation times are greater than T_m. Deformation is essentially elastic for timescales less than T_m. If an impact generates shear stresses of over 10^4 bars (10^3 MPa), strain rates in an olivine mantle range from 10^{-4} to 10^{-2} /s for mantle temperatures of 800-1000°C (10). These values translate to Maxwell times on the order of 1-100 seconds. Because mantle flow requires that the duration of impact exceed T_m, only large, low-velocity (5-6 km/s) impactors (which have impactor penetration times of several tens of seconds (8)) are likely to induce such a viscous mantle response. The range of expected impact velocities at Mars encompasses such low velocities; therefore, subduction of significant crustal sections by large impacts is not impossible on Mars provided that a viscous mantle exists at the time of impact (see 11 for further discussion).

The depth to which crust can be subducted depends on the duration of the impact and T_m. For impact durations equal to T_m, viscous mantle deformation will be of the same magnitude as the elastic deformation associated with transient cavity formation. If we define d as the depth of the transient cavity (roughly the depth of penetration of the projectile (diameter, D_p) into the target), we therefore expect mantle flow to depths of ~D_p beneath the base of the transient cavity. For impact durations that approximate T_m, the region of mantle flow approaches the scale of the displaced flow in the transient cavity. The central crustal section under the impact thus may remain near the base of the transient cavity, thereby leading to rebounded crustal material embedded in a floor of mantle rocks. If the duration of the impact is significantly greater than T_m, however, such material can penetrate the mantle to depths of several D_p and we propose that mantle flow will engulf this displaced crustal section outright. Since the crust tops the subducted section, we model the depth of crustal subduction with a range of ~ $0.5D_p$ to $2D_p$ for impact durations exceding T_m. If d is of the order of the impactor diameter, then subduction depths fall between 100 and 400 km for a projectile 200 km in diameter.

Mantle Evolution: Unlike the fairly continuous plate subduction process observed on Earth, impact subduction is an episodic process which can affect only random and isolated regions of a planetary mantle. The long term effects of continental subduction (e.g., repeated passage of melts

into island arcs or convection beneath back arc basins) are thus unlikely to be associated with impact subduction. Moreover, mantle cooling associated with subduction of cold lithospheric plates also should not occur for impact subduction due to both shock heating and shear deformation of the subducted section. To first order, this subducted crust is presumed to be in thermal equilibrium with normal mantle temperatures at the time of emplacement. Although such a view is proabably over simplistic, the evolution times derived below can be regarded as indicative of the relative time scales required to achieve various mantle states.

Injection of crustal material into the mantle by impact affects both the thermal evolution and subsequent partial melting of the adjacent mantle section. If we assume a subducted crustal component analagous to average terrestrial crust in radiogenic element contents, at 4.0 Ga such material produces heat at a rate of ~43200 J/kg/Ma (12). For subduction to 10 kb pressure and an initial temperature of 1000°C, such heat production begins to melt andesite in ~4 Ma, basalt in ~6 Ma and induces total equilibrium melting of a crustal block in some 9–11 Ma. If fractional melting is considered, given the melt-compatible nature of radiogenic isotopes, most of the heat sources would escape soon after the onset of melting and reduce the total extent of melting. Significant mantle melting is unlikely in this sequence since ~16 Ma are needed to achieve lherzolite melting temperatures outside a subducted block and most of the crustal melts would have escaped by this time. Therefore, partial melts should be silicic or crustal in composition 5–10 Ma after subduction.

Melting of embedded crustal material, however, also can influence the long term thermal evolution of the mantle. Since a fraction of melt is trapped along grain boundaries and in pore spaces during porous flow, not all the melt derived from a subducted block will escape from the mantle. If we approximate the effects of this melt fraction on mantle composition by mixing a disseminated crustal component into the mantle, even for mantle–crust ratios of 100:1 such mixing can double the abundances of heat producing elements in the mantle. This added component then gives rise over time to an anomolously warm mantle region and eventually can induce mantle partial melts some 100–500 Ma after the subduction event.

Finally, subduction can induce mantle melts on shorter time scales through the subduction of volatile concentrations. Although water is unlikely to be a major constituent of the crustal section as a whole, water and ice on early Mars were concentrated in the near surface region. If we postulate an ice–filled regolith 500 m thick with 25% porosity, subduction under a 100–km radius projectile could subduct over 1000 km^3 of water. Impact pressures are likely to vaporize this component during subduction. If the projectile caps the subducted section and drives it into the mantle (see 11), however, this vapor phase may not escape into the transient cavity and will be concentrated near the top of the crustal section after subduction. Addition of such a vapor phase to surrounding mantle compositions significantly reduces the solidus temperatures and, at 1000°C and 10 kb, can initiate mantle melting immediately. Thus subduction of a volatile–rich crustal layer can initiate mantle melts soon after impact with associated fluid–rich and volatile phases possibly resembling kimberlites.

Conclusions: Large, low velocity impacts may inject significant crustal sections into a planetary mantle, but this process will be most efficient if the mantle yields viscously around impact–driven subsidence. The depth of subduction is dependent on the relative scale of impact and mantle flow regimes, but can achieve depths of over 100–200 km for projectiles over 100 km in radius. The effects of such subduction on mantle evolution are unlike those observed in terrestrial subduction zones and primarily reflect the effects of subducted volatile and radiogenic isotope concentrations. Escape of vapor into the mantle should produce kimberlite–like mantle melts soon after impact. Crustal melts develop some 5–10 Ma after impact and enrich higher mantle regions in radiogenic isotopes. Finally, isotopic heating of this enriched mantle may lead to renewed mantle melting several hundred million years after the original impact event.

REFERENCES: 1) Gault, D.E. et al (1968) In *Shock Metamorphism of Natural Materials* (R.M. French and N.M. Short, eds.) p. 87–99. 2) Stoffler, D. et al (1975) *J. Geophys. Res. 80*, p. 4062–4077. 3) Dence, M.R. et al (1977) In *Impact and Explosion Cratering* (D.J. Roddy, R.O. Peppin and R.B. Merrill, eds.) p. 247–275. 4) Schultz, P.H. et al (1981) *Proc. Lunar Planet. Sci. 12A*, p. 181–195. 5) Croft, S.K. (1981) *Proc. Lunar Planet. Sci. 12A*, p. 207–225. 6) Grieve, R.A.F. (1981) *Proc. Lunar Planet. Sci. 12A*, p. 37–57. 7) Wichman, R.W. and Schultz, P.H. (1989) *J. Geophys. Res.*, in press. 8) Schultz, P.H. (1988) In *Mercury* (F. Villas, C.R. Chapman and M.S. Matthews, eds.) p. 274–335. 9) Melosh, H.J. (1989) *Impact Cratering*, p. 156. 10) Stocker, R.L. and Ashby, M.F. (1973) *Rev. Geophys. Space Physics 11*, p. 391–426. 11) Schultz, P.H. and Wichman, R.W. (1990), this volume. 12) Bott, M.H.P. (1982) *The Interior of the Earth*, p.272.

CONSTRAINTS ON MAGMA CHAMBER DEPTH OF THE OLYMPUS MONS VOLCANO, MARS; *M.T. Zuber*, Geodynamics Branch, Code 621, NASA/Goddard Space Flight Center, Greenbelt, MD 20771, *and P.J. Mouginis-Mark*, Planetary Geosciences Division, Hawaii Institute of Geophysics, University of Hawaii, Honolulu, HI 96822.

The summit caldera of Olympus Mons exhibits one of the clearest examples of tectonic processes associated with shield volcanism on Mars [1,2]. Within the 80 km diameter structure are six nested craters that indicate that the volcano edifice has undergone multiple collapse episodes [1]. Also found within the caldera are numerous wrinkle ridges and graben. Analysis of the topography of the caldera as derived from stereophotogrammetry [3] shows that the central portion of the largest crater, where the majority of the ridges are located, represents a topographic low, while the crater perimeter, which is characterized by circumferential graben, forms a topographic high (Figure 1). The relationship of the summit topography to the tectonic features, in combination with photogeologic evidence for basalt-like resurfacing of the caldera floor [4], is believed to indicate that a large lava lake has cooled and subsided as magma from the underlying chamber was withdrawn by flank eruptions [1].

If the tectonic features within the caldera developed in response to subsidence associated with magma withdrawal, then these features contain information about the nature of the subsurface magmatic reservoir. Specifically, the radial locations of the ridges and graben can be used to constrain magma chamber depth. We have analyzed Viking orbiter images of the Olympus Mons caldera and conclude that it is reasonable to assume that tectonic features within it could have formed due to subsidence. We thus attempt to constrain the depth of the magmatic reservoir by calculating radial surface stresses (σ_{rr}) corresponding to a subsurface pressure distribution representing an evacuating magma chamber. We compare the resulting stress patterns to the radial positions of compressional (ridges) and extensional (graben) features within the caldera.

We solve the problem by employing a finite element approach. Figure 2 shows a sample grid that represents a cross-section of the volcano in the vicinity of the summit. An axisymmetric geometry and linear elastic material properties are assumed. The magma chamber is modeled as an elliptically-shaped source with a Young's Modulus that may be the same as or different than that of the surrounding material. Nodes within the ellipse are characterized by a stress condition that represents an instantaneous uniform pressure drop. The horizontal dimension of the chamber is assumed to be similar to that of the caldera, as observed for Kilauea [5]. For the model shown, the following boundary conditions are imposed: vanishing horizontal (u) displacements at the center of symmetry (left boundary) of the volcano; vanishing vertical (w) displacements at depths much greater than the crater radius (bottom boundary); and vanishing horizontal and vertical displacements at radial distances far from the crater rim (right boundary). Numerical analyses were performed to assure that solutions were not sensitive to the far field boundary conditions.

Examples of normalized radial stress distributions for a series of magma chamber depths are shown in Figure 3. Negative stresses are compressional and positive stresses are extensional. The state of stress as inferred from the radial locations of ridges and graben in the largest crater in the Olympus Mons caldera changes from compression to extension at a radial distance from the crater center of approximately 0.5-0.75R, where R is the crater radius (32 km). The corresponding best-fit pattern of stresses indicates that the top of the magma chamber at the time of subsidence was located at a depth of less than the crater radius (best fit range approximately $8 \leq d \leq 16$ km), and was therefore within the volcanic construct. This result, which is in agreement with our previous analysis that treated the chamber as a simple horizontal line source [6], is relatively insensitive to both the vertical dimension of the chamber and the difference in Young's Modulus between the chamber and surroundings. A similar depth/radius ratio is observed for the magma chamber in the Kilauea caldera [5], which would suggest a gross similarity of internal structure of the two shields.

We are currently examining other plausible magma chamber geometries and are considering modifications of predicted radial stress patterns due to factors [e.g. 7] in addition to magmatic withdrawal. We thus hope to further constrain the depth of the magma chamber and to better understand the implications for the internal structure of Olympus Mons.

References: [1]Mouginis-Mark, P.J., *Proc. Lunar Planet. Sci. Conf. XII*, 1431-1447, 1981. [2]Mouginis-Mark, P.J., L. Wilson, and M.T. Zuber, submitted to *Mars*, University of Arizona Press, Tucson, 1989. [3]Wu, S.S.C., P.A. Garcia, R. Schafer, and B.A. Skiff, *Nature, 309*, 432-435, 1984. [4]Greeley, R., and P.D. Spudis, *Rev. Geophys., 19*, 13-41, 1981. [5]Ryan, M.P., J.Y.K. Blevins, A.T. Okamura, and R.Y. Koyanagi, *J. Geophys. Res., 88*, 4147-4181, 1983. [6]Zuber, M.T. and P.J.

Mouginis-Mark, *Proc. MEVTV Confererence on Tectonic Features on Mars*,, LPI, Houston, 1989. [7]Thomas, P.J., S.W. Squyres, and M.H. Carr, *J. Geophys. Res.*, in press, 1989. [8]Mouginis-Mark, P.J., and A. Mathews, *EOS Trans. Am. Geophys. Un.*, *68*, 1342, 1987.

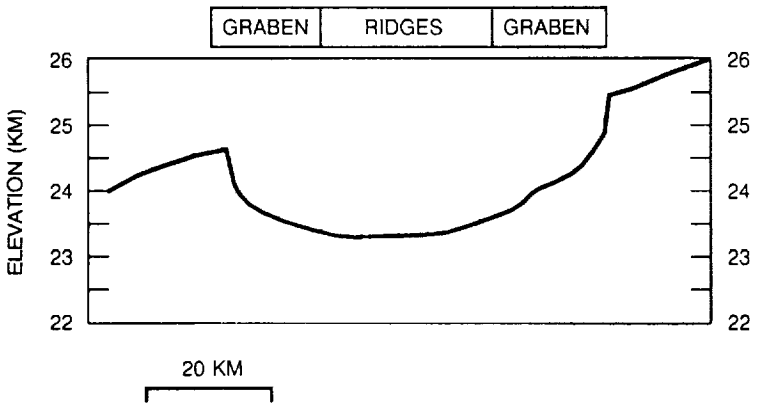

Figure 1. Topography and radial distribution of ridges and graben in the largest crater of the Olympus Mons caldera complex (after [8]). The profile traverses only the oldest of the six craters in the attempt isolate tectonic features associated with a single deformational episode.

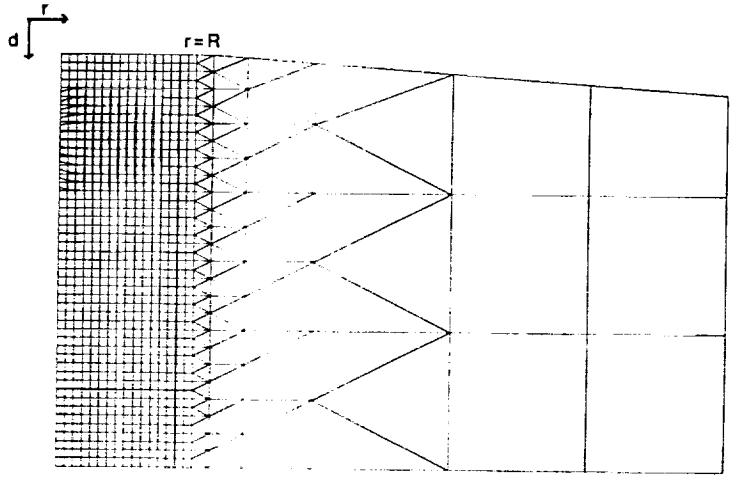

Figure 2. Finite element grid representing a cross-section of the volcanic construct before and after deformation for a magma chamber at depth d=0.25R. The crater rim is located at r=R.

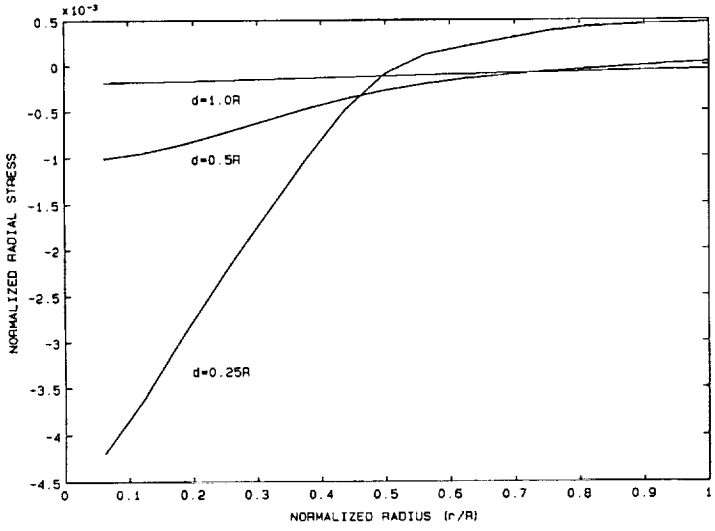

Figure 3. Plot of normalized radial surface stress (σ_{rr}) as a function of distance (r/R) from the crater center at a range of depths (d) beneath the surface. Assumes an elliptical source with semi-major axis equal to the crater radius (R). Negative stresses are compressional and positive stresses are extensional.

List of Workshop Participants

Jayne Aubele
Department of Geological Sciences
Brown University
Box 1846
Providence, RI 02912

Nadine G. Barlow
Code SN21
NASA Johnson Space Center
Houston, TX 77058

Connie Bertka
Department of Geology
Arizona State University
Tempe, AZ 85287-1404

Roger G. Burns
54-816
Massachusetts Institute of Technology
Cambridge, MA 02139

Joy Crisp
Mail Stop 183-501
Jet Propulsion Laboratory
4800 Oak Grove Drive
Pasadena, CA 91109

David Crown
Department of Geology
Arizona State University
Tempe, AZ 85287-1404

Larry Crumpler
Department of Geological Sciences
Brown University
Box 1846
Providence, RI 02912

Shanaka de Silva
Lunar and Planetary Institute
3303 NASA Road 1
Houston, TX 77058

Sarah A. Fagents
Environmental Science Division
Lancaster University
Lancaster LA1 4YQ
England

Jim Garvin
Code 621
NASA Goddard Space Flight Center
Greenbelt, MD 20771

Ron Greeley
Department of Geology
Arizona State University
Tempe, AZ 85287-1404

John Holloway
Department of Geology
Arizona State University
Tempe, AZ 85287-1404

Marie Johnson
Department of Geological Sciences
Brown University
Box 1846
Providence, RI 02912

John Jones
Code SN21
NASA Johnson Space Center
Houston, TX 77058

Susan Keddie
Department of Geological Sciences
Brown University
Box 1846
Providence, RI 02912

Laurie Leshin
Mail Code 170-25
California Institute of Technology
Pasadena, CA 91125

John Longhi
Lamont-Doherty Geological Observatory
Palisades, NY 10964

Rosaly Lopes
Mail Stop 183-501
Jet Propulsion Laboratory
4800 Oak Grove Drive
Pasadena, CA 91109

Baerbel K. Lucchitta
U.S. Geological Survey
2255 North Gemini Drive
Flagstaff, AZ 86001

Patrick J. McGovern
54-521
Massachusetts Institute of Technology
Cambridge, MA 02139

Henry J. Moore
Mail Stop 946
U.S. Geological Survey
345 Middlefield Road
Menlo Park, CA 94025

Peter Mouginis-Mark
Planetary Geosciences
University of Hawaii
2525 Correa Road
Honolulu, HI 96822

Vivian Pan
Department of Geology
Arizona State University
Tempe, AZ 85287-1404

Ian Ridley
U.S. Geological Society
Denver Federal Center
Box 25046, Mail Stop 973
Denver, CO 80225

Cordula Robinson
ULO Observatory Annexe
33-35 Daws Lane
London NW7 4SD
England

Mark Robinson
Planetary Geosciences
University of Hawaii
2525 Correa Road
Honolulu, HI 96822

Scott Rowland
Planetary Geosciences
Hawaii Institute of Geophysics
2525 Correa Road
Honolulu, HI 96822

Mac Rutherford
Department of Geological Sciences
Brown University
Box 1846
Providence, RI 02912

Dave Scott
U.S. Geological Survey
2255 North Gemini Drive
Flagstaff, AZ 86001

Sean C. Solomon
54-522
Massachusetts Institute of Technology
Cambridge, MA 02139

Frank J. Spera
Department of Geological Sciences
University of California
Santa Barbara, CA 93106

Ed Stolper
Department of Geology
Mail Code 170-25
California Institute of Technology
Pasadena, CA 91125

Robert Wichman
Department of Geological Sciences
Brown University
Box 1846
Providence, RI 02912

Lionel Wilson
Environmental Science Division
Lancaster University
Lancaster LA1 4YQ
England

Maria Zuber
Code 621
NASA Goddard Space Flight Center
Greenbelt, MD 20771

NOTES